UNIVERSITÀ DEGLI STUDI DI TRENTO
Dipartimento di Fisica

Corso di Laurea Magistrale in Fisica

Tesi finale

Optical characterization of ferroelectric plasmonic devices

Relatore:
Prof. Paolo Bettotti

Correlatore:
Dr. Magnus Jonsson

Laureando:
Giancarlo Cincotti

Anno Accademico 2017-2018

Acknowledgements

I would like to express my sincere gratitude to my co-supervisor Magnus Jonsson for all the support and the prolific discussions we had. I would like to thank my supervisor Paolo Bettotti for the suggestion on my Thesis and for the help.

My sincere thanks to Mina Shiran Chaharsoughi for supporting me and teaching how to realize the devices, to Stefano Rossi for all the help with the simulations and to all the Loe people for the amazing atmosphere.

I would like to thank my family for support and helpfulness and Rachele Casarotto for her love and patience.

Abstract

In this work we investigated the optical effect of coupling a ferroelectric polarized material to a plasmonic nanostructure.

It has been demonstrated that the excess or defect of charge, in a metallic nanostructure, modify the localized surface plasmonic supported resonance. Polarizing the ferroelectric material a surface charge is created in contact with the plasmonic nanostructure. The surface charge can then modify the charge concentration, but no works have been done to investigate this phenomenon.

Hybrid plasmonic-ferroelectric device was made using hole-mask colloidal lithography. These devices are made of a thin layer of Poly(vinylidenefluoride - trifluoroethylene) ferroelectric copolymer coupled to a gold nanodisks array. The device is enclosed between two electrodes to polarize the material in two different directions.

To change polarization we used a source-meter while to measure the optical extinction and reflection spectra we used a spectrometer. A LabView program was made to synchronously acquire data from those two instruments.

The extinction and reflection spectra were initially studied to distinguish the optical phenomena and then compared with finite-difference frequency-domain simulations.

Devices were stimulated electrically and the spectral evolution in time was monitored following the different peaks shift. We used a centroid- based algorithm to determine the peak position. We made statistics on the results to find peak shifts between two polarization directions of the ferroelectric material.

In conclusion we noticed a Fabry-Perot cavity effect supported by the device and a difference in the plasmonic peak position for two polarizations of the ferroelectric material.

Contents

Part I

Aim of the Thesis

Until now no research have observed the interaction between polymeric ferroelectric materials coupled on plasmonic nanostructures.

In this Thesis a coupled plasmonic-piezoelectric device is used to study the effect of different polarization states on the optical proprieties of gold nanodisks and nanoholes arrays.

It has been proven that, for plasmonic nanostructures, an excess of charge can cause a plasmonic resonance shift due to a change in carrier concentration.

The ferroelectric P(VDF-TrFE), when polarized, present a surface charge modification. This charge is located on the interface between this ferroelectric material and the plasmonic resonant system, and can cause a modification in the carrier density of the used nanostructures.

With this work we investigate, experimentally and with the help of simulations, the optical response of hybrid plasmonic ferroelectric devices, focusing on different supported phenomena. We also focus on the shift of various resonant peaks in the material optical spectrum, which are correlated to different electrical stimulation and polarization states.

Part II

Introduction and Theory

In the last twenty years, with advances in the fabrication techniques, characterization methods and simulations capabilities, the field of Plasmonics has been constantly growing, offering new great opportunities to different fields.

For plasmon we refer to the coherent oscillation of conduction band electron gas into a conductive material. Although semiconductor nanocrystals plasmons has been studied [FSJ14], plasmonics has been developed mainly with noble metals, due to resonant peaks close to the visible region, then excitable by common optical sources, and low losses [LLH07].

Dependently on the dispersion relation of this kind of oscillations we can distinguish between bulk plasmons, which propagates through the material, and surface plasmons (SPs), which propagates on the interface between a metal and a dielectric. A particular type of SPs are the localized surface plasmons (LSPs), resonant modes where the energy carried by the electric field is confined in a specific volume.

The interaction between metallic nanoparticles and light can be described by LSP which, due to its localized nature, do not require a phase matching condition on the momentum carried. This implies, unlike in the case of SP, that light can directly couple in nanoparticles or nanostructures, resulting in strong field enhancement and localization.

During research expansion of LSPs in nanoparticles, many applications came out. A non exhaustive list should include Surface Enhanced Raman Spectroscopy (SERS), where Nie et al. increased the resolution of Raman spectroscopy with the field enhancement effect of Ag nanoparticles [NE97]. Plasmonic sensing is performed also on catalytic reaction dynamic, where the absorbate coverage on support material can be monitored due to a LSP resonance shift in gold nanostructures [Lar+09].

Tuning the geometry of nanoparticles or nanostructures allow different plasmonic modes to coexist and mix due to interference phenomena. This mixing results in Fano resonances [Luk+10], used to enhance selectively both peaks in Coherent Anti-Stokes SERS (SECARS) [He+16], or electromagnetically induced transparency (EIT), providing a sharp transparency window for selective plasmonic sensing [Liu+10].

Chapter 1

Plasmonics fundamentals

In this Thesis we are going to study the behaviour of plasmonic nanostructures that supports localized surface plasmonic resonance, a coupled oscillation between electromagnetic field and electron density that is localized and resonate in a defined volume. In more details we are going to modify the conditions of the surrounding medium, composed of a ferroelectric material. To give meaning to that changes it necessary to describe the observed phenomena with a theoretical treatment, that is possible deriving plasmonic waves from the Drude model in metals. This theory, under approximations, can be restricted to localized resonances, and gives a hint on experimental phenomena that we can observe.

1.1 Optical properties of metals

Metals form usually crystalline aggregates, which contain small crystals with random orientation. This allow an electromagnetical treatment as isotropic media.

Imposing the presence of free charge and current density we have a complex absolute permittivity $\hat{\epsilon}$ and a complex refractive index $\hat{n}$

$$\hat{\epsilon} = \epsilon + i\frac{4\pi\sigma}{\omega} \tag{1.1}$$

$$\hat{n} = n(1 + i\kappa) \tag{1.2}$$

$$\hat{n}^2 = \mu(\epsilon + i\frac{4\pi\sigma}{\omega}) \tag{1.3}$$

where σ is the conductivity, μ the magnetic permeability, κ the attenuation index and σ the conductivity.

A characteristic of metals is the Joule irreversible phenomena that converts kinetic electrons energy to heat. This lead to the strong absorption, small field penetration, high reflectively and opaque appearance [BW99], according to a complex wave vector providing amplitude attenuation.

Despite plasmons shows quantum phenomena such as interference between modes, a satisfactory description can be derived from a simple model based on kinetics and classical electrodynamics.

1.1.1 Drude Model

Drude model [Dru00] is derived from the kinetic theory of gas and describes electrons in a metal as a cloud of free to move non interacting particles surrounding positively charged ions. Those ions, composed by nucleus and core electrons, are assumed to be steady due to the big mass in comparison to electrons. The first assumption to apply kinetic gas theory is that electrons are not perturbed, during their motion, neither by electronic nor by ionic field during their motion. They travel in straight lines between collisions when the interaction with the nucleus happens. After colliding with ions, electrons change velocity abruptly, with a characteristic time between collisions τ. The second assumption regards thermodynamics and affirms that the only way that electrons have to lose energy is through collisions. After a collision, the electron has a completely uncorrelated kinetic energy, related to the local surrounding temperature.

We can now set Eq.(1.4) for the dynamics of electrons

$$m\ddot{\mathbf{x}} + m\gamma\dot{\mathbf{x}} + e\mathbf{E} = 0 \tag{1.4}$$

where x is the displacement of the electrons from ions, m is the effective mass of the electrons, $\mathbf{E}$ is the stimulating electric field, and γ is the damping constant, due to collisions.

We can move to Fourier reciprocal space in ω and stimulating the system with an harmonic field. We use a macroscopic definition of polarization related to electrons displacement, $\mathbf{P} = -Nex$, where N is the electron density. We find an expression for σ to substitute in 1.1, and express the ω dependent dielectric function

$$\epsilon(\omega) = \epsilon_\infty(1 - \frac{\omega_p^2}{\omega^2 + i\gamma\omega}) \tag{1.5}$$

where ω_p is the resonance frequency of free electrons in the media. For $\omega^2 >> \gamma^2$ and $\omega < \omega_p$ (condition providing $\hat{\epsilon}$ negative and real), the dielectric constant and the plasma frequency can be approximated as

$$\epsilon(\omega) = 1 - \frac{\omega_p^2}{\omega^2} \tag{1.6}$$

$$\omega_p^2 = \frac{Ne^2}{\epsilon_0 m} \tag{1.7}$$

From the model, if we use $\omega > \omega_p$, the real part of $\hat{\epsilon}$ become positive and, for sufficiently large ω, $\hat{\epsilon} \approx \epsilon$. In this case the metal is like a dielectric, and is expected to be transparent. Despite this, interband transitions occur, and experimentally observed behaviour differs for energy higher than 1.8 eV. A phenomenological model that maintains Drude-form accounts this phenomena [DKD16] [BW99].

1.1.2 Propagating surface plasmon polariton (SPP)

With the help of the Drude model, describing free electrons behaviour into metals, is is possible to set the equations that describe propagating plasmonic waves localized on the surface between metal and dielectric. Some metallic nanostructures present an extended surface that have an interface between metal and dielectric,

therefore representing an ideal substrate for the study of SPP.

To describe SPPs we set up a system consisting in two dielectric media interfaced in $z = 0$. They have frequency dependent dielectric constants ϵ_1 and ϵ_2. We start now from Maxwell equations in uniform and non-magnetic media, without sources [Jac99]. We use index $i = 1$ for $z < 0$ and $i = 2$ for $z > 0$.

$$\nabla \cdot (\mathbf{E}_i \epsilon_i) = 0 \tag{1.8}$$

$$\nabla \cdot \mathbf{H}_i = 0 \tag{1.9}$$

$$\nabla \times \mathbf{E}_i = -\frac{1}{c}\frac{\partial}{\partial t}\mathbf{H}_i \tag{1.10}$$

$$\nabla \times \mathbf{H}_i = \epsilon_i \frac{1}{c}\frac{\partial}{\partial t}\mathbf{E_i} \tag{1.11}$$

Normally it is possible to solve those equations for a propagating wave in the bulk, but we impose a solution propagating in x direction. By taking into consideration boundary conditions on fields we have to deal with TM waves. We can write fields in the following form, where $k_{i,j}$ is the wave vector, i the material and j the direction.

$$\mathbf{E}_i = (E_{i,x}, 0, E_{i,z}) e^{i(k_{i,z}z + k_{i,x}x - \omega t)} \tag{1.12}$$

$$\mathbf{H}_i = (0, H_{i,y}, 0) e^{i(k_{i,z}z + k_{i,x}x - \omega t)} \tag{1.13}$$

Inserting this field forms into Maxwell equation, and applying boundary conditions

$$\frac{k_{1,z}}{\epsilon_1} = \frac{k_{2,z}}{\epsilon_2} \tag{1.14}$$

$$k_{1,x} = k_{2,x} = k_x \tag{1.15}$$

$$k_x = \frac{\omega}{c}\sqrt{\frac{\epsilon_1 \epsilon_2}{\epsilon_1 + \epsilon_2}} \tag{1.16}$$

We require propagating waves in x direction and localized in z direction. We

obtain then a condition on real and imaginary part of wave vector

$$\Im(k_x) = 0 \quad \Re(k_z) = 0 \tag{1.17}$$

Now we use the Drude result for metals 1.6 in material 1, and vacuum for material 2. The resulting dispersion relation is the following.

$$k_x = \frac{\omega}{c}\sqrt{\frac{\omega^2 - \omega_p}{2\omega^2 - \omega_p}} \tag{1.18}$$

This shows that a propagating wave, localized near the interface and exponentially damped in amplitude, is supported by a metal coupled to a dielectric material.

1.1.3 Localized surface plasmon polariton (LSPP)

Gold nanodisks have been used in our study to observe a localized plasmonic resonance. The structure doesn't support SPP, because there is not the possibility for a plasmonic wave to propagate, but it allows the presence of a resonant mode called LSPP.

LSPP are resonance modes due to the coupling between conductive electron plasma excitation in metal and an electromagnetic field, restricted to a specific volume It is possible to excite them into sub-wavelength nanostructures and they are characterized by strong field enhancement near to the surface and high losses with frequencies near to the resonance frequency [Pit+07]. In this case coupling with an incoming source do not require phase matching condition, because the LSPPs are not propagating waves, then LSPP can be excited directly illuminating the nanostructures with a light source at the resonant frequency.

Although plasmonic nanostructures can be created in many different shapes, simple geometries (e.g. sphere) are needed for the analytic description. A successful result can be obtained for a spherical particle immersed in an electromagnetic field, using the quasistatic approximation. This approximation considers the particle much smaller than the wavelength and is applicable for objects smaller than 100 nm[Mai07].

The polarizability of a metallic nanoparticle of radius a is

$$\alpha = 4\pi a^2 \frac{\epsilon - \epsilon_m}{\epsilon + 2\epsilon_m} \tag{1.19}$$

In order to maximize the function, we ask

$$\Re(\epsilon) = -2\epsilon_m \tag{1.20}$$

That is called Fröhlich condition.

An analytic solution is achievable also for ellipsoidal geometries [BH83]. The polarization on the i-th axis is

$$\alpha_i = 4\pi a_1 a_2 a_3 \frac{\epsilon(\omega) - \epsilon_m}{3\epsilon_m + 3L_i(\epsilon(\omega) - \epsilon_m)} \tag{1.21}$$

$$L_i = \frac{a_1 a_2 a_3}{2} \int_0^\infty \frac{dq}{(a_i^2 + q)\sqrt{(q + a_1^2)(q + a_2^2)(q + a_3^2)}} \tag{1.22}$$

with L_i a geometrical factor and a_i semiaxes

Many nanostructures can be approximated to spheroids (ellipsoids with two equal semiaxes). In this case the main result is the presence of two different resonant modes, associated to distinct orientations. If the spheroid's mode associated to the longest axis is red shifted with respect to the mode related to a sphere (with radius equal to the major semiaxis).

For ellipsoidal nanoparticles with dimensions comparable with the wavelength, we need to consider spatial retardation effects of the electromagnetic wave in the nanoparticle volume.

Mie theory of scattering provide a valid instrument to predict the behaviour in terms of resonant modes. This theory gives a solution for Maxwell equation expanding scattered fields in vector spherical harmonics. In general the result is a red shift of the resonant peak with growing particle size [Mai07].

A consequence for our study, that consider gold nanodisks, is that the resonance is tunable in wavelength changing the thickness of the metal that is deposit without changing particle size. In our case we used a thickness of 30 nm, and a diameter of 160 nm, that brings the resonance in the visible, at 780 nm

Regarding the damping process, two different nanostructure's responses are possible. The first is a radiative path consisting in the creation of photons at the resonant frequency, and the second is the creation of electron and hole pairs with intraband and interband excitation. To relate these processes to the absorbance of the material a relaxation time for both processes is used, which can be related to the quality factor of the resonator $Q = E_{res}\frac{T}{2\hbar}$, where T is called dephasing time. For gold nanospheres of 200 nm the main contribution to the damping process is associated to non radiative processes, with $T_{nr} = (8.1 - 9.0) \cdot 10^{-15}s$ and $T_{rad} = (7 \cdot 10^{-15}s - 8 \cdot 10^{-13}s)$ [HH85].

Ordered and short range ordered arrays of nanoparticles

Optical proprieties of nanoparticles are usually experimentally determined by grouping them together in a 1d, 2d or 3d matrix of similar nanoparticles, with a low dispersion in size and shape.

In our case the plasmonic surface present an array or randomly distributed gold nanodisks, created by colloidal lithography. This allows the characterization by common optical techniques because we observe the plasmonic effect on a broad area.

If the spacing is much less than the wavelength of the nanoparticle, dipolar modes can interact and couple together, resulting in an enhanced field in the space between nanoparticles, as used for enhanced coherent antistokes Raman spectroscopy [He+16].

It is possible to show that for a linear array of small (diameter 50 nm) gold nanoparticles, considered as point-like dipoles, two opposite resonance shifts occur with two different polarizations, vanishing for separation larger than 125 nm [Mai+02]. This set a limit in the near field interaction between nanoparticles.

Coupling can also occurs between more distant nanoparticles, in this case we refer to far field coupling given by nanoparticles scattered fields. The grating effect in periodically spaced 1d or 2d matrix allows coupling with spacing comparable to the wavelength. This collective oscillations affect the resonance wavelength and width, related to the decay time of the plasmon, showing different radiative and non radiative behaviours for different spacing [Lam+00].

For randomly distributed 2d array of nanoparticles, with short range order, collective oscillations instead are not relevant. The nanoparticles act essentially as single scatterers and absorbers without dipole interaction [Lam+00] [HKS03]. In our study we use randomly distrbuted nanodisks with short range order and 325 nm spacing as peak in the radial distribution function [Shi+18]. This spacing and the random distribution avoid collective effects.

It is possible to describe the optical characteristics of array of metallic nanoparticles using this wavelength dependent coefficients: Transmission(T) , Reflection (R), Absorption (A), Extinction (E), Scattering (S). Extinction describes the sum of absorption, reflection and scattering, both in forward (S1) and backward direction (S2), and it is related to the incoming light intensity,

$$E = A + S = 1 - \frac{I}{I_0} \tag{1.23}$$

With I the transmitted light beam passing through the array and I_0 the incoming light beam.

Effects of geometry on gold nanodisks LSPR

Considering different nanoparticles geometries, nanodisks represent a convenient base to obtain strong plasmonic effects. Usually nanodisks present a dipolar excitation mode strongly dependent on the size. The diameter dependence of the resonance peak is derivable analytically from the models described in chapter 1.1.3. The assumption is that nanodisks are assimilable as spheroids, with $h << D$ (h height, D diameter) and dimensions $h = a_1/2, D = a_2/2$.

The dependence of the resonant peak on particle diameter is experimentally demonstrated by Zorich et al. [Zor+11] and it is

$$\omega_{LSPR}^2 = \frac{3Lc^2}{a_1 a_2} \tag{1.24}$$

Increasing the radius R, interband absorption processes decrease their incidence, leaving room for scattering mechanism. Considering 20 nm thick nanodisks, the crossover radius results to be $R_c = 150nm$ [LKZ07].

Effects of charge density on gold nanodisk's LSPR

For this work we use hybrid plasmonic-ferroelectric device. An array of gold nanodisks is placed in contact with a ferroelectric material, that can be polarized. The polarization of the material creates a surface charge density on the material. In this chapter we report the effect that a modification of the electron distribution induces on LSPR optical properties.

Excess or defect of charge carriers in plasmonic structure result in a shift in the LSPR mode called CIPS (Charge Induced Plasmon Shift). CIPS has been shown with nanoparticles in colloidal solution by adding a reducing agent or by immersing a cathode and providing a voltage [Mul+06].

An increase of free electron density cause a blueshift in extinction spectra and a decrease cause a redshift due to the variation of carrier density in Drude model. Theoretically the problem has been studied by Liow et al. analyzing different metallic nanoparticles and coupled metallic nanoparticle [Lio+14].

A correlation has been found between CIPS and aspect ratio of gold nanorods and nanodisks. Higher aspect ratio, intended as the ratio between diameter and length in nanorods and between height and diameter in nanodisks, shows stronger blueshift when charge density is increased.

To describe analytically this shift it is possible to consider a modified quasistatic Drude theory, where an additional charge density ΔN is added the the characteristic charge concentration N.

Following the derivation from Juluri et al. [Jul+08], a resonant wavelength $\lambda_{\Delta N}$ with dependence on the electron density is found. The derivation uses the resonant condition for nanodisks, imposing maximum value for the polarization in Eq. (1.21) and so a vanishing denominator.

$$\lambda_{\Delta N} = \frac{\lambda_p \sqrt{A_i}}{\sqrt{1 + \frac{\Delta N}{N} - \frac{\gamma^2 A_i}{\omega_p^2}}} \tag{1.25}$$

$$A_i = 1 - \epsilon_m \tag{1.26}$$

Though it is not possible to estimate λ_a for our nanostructures, we can see from the above equations that an increase of the electron density causes a blue shift in the resonance frequency.

Chapter 2

Fabry-Perot cavities

The devices used for this thesis are composed by a permanently polarized ferroelectric thin film. The film is coupled to a plasmonic layer composed by gold nanodisks. In order to polarize the ferroelectric field it is necessary to apply an external electric field. The electric field is generated by two electrodes: the first is made by ITO and resides below the plasmonic nanostructures , while the second is made by gold thin film and is placed on the other face.

A Fabry-Perot cavity is a resonant cavity for electromagnetic waves consisting in two reflective plates with a thin dielectric material in the middle. The geometric characteristic and the specific transmittivity ad reflectivity of the mirrors allow an incident wavefront to constructively interference for specific resonant wavelengths, creating standing waves inside the cavity.

In our case the effect is observed because the layer with nanodisks, representing one mirror, have a not negligible reflectivity, then the gold film create a cavity with the ferroelectric material in the middle.

The resonant condition in Eq. (2.1) is obtained imposing a constructive interference between incoming and reflected waves inside the cavity.

$$k_p = \frac{2\pi}{\lambda_p} = q\frac{\pi}{d} \tag{2.1}$$

where d is the cavity width, q an integer, λ_p and k_p resonant wavelength and wave vector.

The condition on the resonant frequency of Eq. (2.1) is derived considering

the two plates giving a phase shift of π. In the case of thin films and plasmonic nanostructures we expect a modification on that value.

Following the treatment of [ST19] the spectral response is

$$I = \frac{I_{max}}{1 + (2F/\pi)^2} sin^2(\pi\nu/\nu_F) \tag{2.2}$$

$$I_{max} = \frac{I_0}{(1-\nu)^2} \tag{2.3}$$

$$F = \frac{\pi\sqrt{r}}{1-r} \tag{2.4}$$

where I is the transmitted intensity, I_0 the input intensity, F is the finesse, related to the sharpness of the peaks, I_{max} the maximum value of the output intensity, ν the frequency, r the square root of the power losses during one round trip, ν_F the resonant frequencies.

Losses are caused both by the cavity material and by the imperfect reflectance of the mirrors. It is possible to correlate r to the reflectance of the two mirrors and the power attenuation factor

$$r^2 = R_1 R_2 e^{-\alpha_s d} \tag{2.5}$$

In our case the reflectivity of the plasmonic mirror is not comparable to the reflectivity of a thin gold film, then the quality factor of the resonator is lower than for a cavity with two thin film mirrors, causing a broadening of Extinction spectra.

Chapter 3

Piezoelectric and Pyroelectric materials

Non centrosymmetric materials can show peculiar propertes, such as pyroelectricity, piezoelectricity and ferroelectricity. In particular ferroelectric materials are always piezoelectric and pyroelectric and pyroelectric materials are always piezoelectric, but the opposite is not true.

Ferroelectric materials are a class of materials that present a spontaneous electric polarization. This property is related with specific symmetric properties of the crystal structure of the material, and specifically with non-centrosymmetric materials [OCH06].

In comparison to dielectrics, that present a linear polarization with the applied electric field, and paraelectric materials, which show nonlinearities, ferroelectric materials present a non-zero polarization, even without external electric field.

The internal polarization is reversible with a suitable high enough electric field. This leads to a hysteresis cycle, where the polarization depends on the history of the material. Ferroelectric behaviour is shown under a certain Curie temperature, characteristic of each material.

Piezoelectricity is the property of producing electrical charge when a mechanical force is applied. This mechanism is reversible, in the sense that mechanical stress, and so deformation, is achieved when the material is electrically stimulated. This effect derives from the presence of electric dipole moments in the material,

caused by asymmetries in the charge distribution of lattice or molecular groups. Mechanical stress causes a reconfiguration of the material's dipoles, leading to a surface charge, and then to an electric field between the faces.

Pyroelectricity and piezoelectricity can be described by

$$P - P_r^0 = \chi^X \epsilon_0 E + dX + p(T - T_0) \tag{3.1}$$

where P the electric polarization, P_r^0 is the residual polarization, χ^X the free electric susceptibility, p is the pyroelectric coefficient, d the piezoelectric coefficient, E is the electric field, X the stress tensor and T_0 the natural state temperature.

Pyroelectricity and piezoelectricity can be caused by two different mechanisms. The first is a spontaneous polarization that can occur, for example, in a polymeric film. The polarized state is not a thermodynamically stable state and should be treated as a metastable state where charges, at room temperature, are frozen. After heating up the material over the Curie temperature the charges become movable and the material loose its pyroelectric and piezoelectric effect. The second mechanism is related to the heterogeneity of a polymeric non conductive film and the relative presence of embedded charges [WH76].

3.1 P(VDF-TrFE) copolymer films

Poly(vinylidenefluoride-trifluoroethylene) is a co-polymer and ferroelectric material.

We used this material as a film interfaced with plasmonic nanostructures and placed between two conductive films that act as electrodes to polarize the material.

Historically the copolymer is an evolution of P(VDF) Poly(vinylidene fluoride). This material, in nanometric films, after being stretched in ratio 4:1, reach semi crystalline beta phase shown in Fig. 3.1. In this phase the dipoles of the material are aligned and produce a net dipole due to the high electronegativity difference between fluorine and hydrogen [Rua+18]. In this phase PVDF can reach polarizations of 2000 V/cm.

The film is polarized with the so called poling process while being heated at least at 60° [Kaw69]. The poling process consists in applying a suitable strong

electric field in order to force dipoles orientation in one direction. The ferroelectric behaviour of that polymer is due to the non vanishing dipole domain orientation also when the field is removed, leading to a pyroelectric and piezoelectric effect [FDF80]. Piezoelectric effect can be noticed from Fig. 3.1: if an electric field is applied through the structure, it will attract or repel H side and F side, depending on the orientation of the field, causing a stress in the material.

PVDF polymer requires to be stretched on a ratio 4:1 before poling. To overcome this limitation in some points $VF_2(CH_2 - CF_2)$ is replaced by $VF_3(CH - CF_3)$ creating a co-polymer. Considering the differences in size of the two polymers, the co-polymer will crystallize directly in beta phase [Ueb01], resulting more convenient for applications.

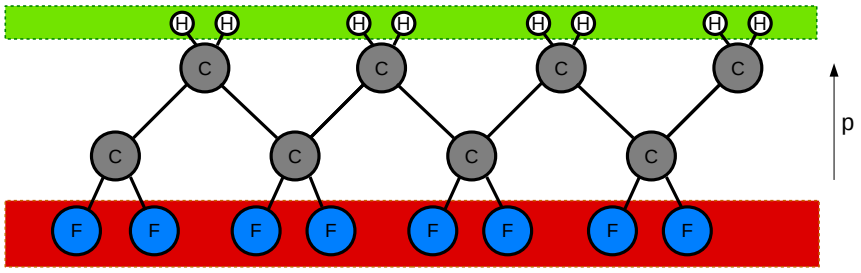

Figure 3.1: Structure of PVDF semi crystalline polymer. Green area is positively charged and electropositive due to the presence of H atoms. Red area, on the other hand, is negatively charged and electronegative. Source: [13]

In our case the application of a voltage to polarize the material cause a stretching of the film and a variation in the supported mode of the Fabry-Perot cavity. To estimate the stretching we use $d = -30pmV^{-1}$ [Kat+16].

Part III

Experimental methods

To achieve the results obtained this Thesis, the experimental work is divided in different sections.

In this experimental section we describe the techniques used to analyze experimentally the behaviour of plasmonic nanostructures when coupled with differently polarized material.

First, the devices were produced following a specific procedure that involves hole-mask colloidal lithography [Fre+07] and physical vapour deposition previously described in literature [Shi+18].

To perform the required measurements the instrumentation were interfaced to a PC via LabView, in order to acquire time correlated data from the optical and the electrical part. Another program was written to analyze the acquired data and show it in a convenient way.

The devices were optically probed measuring extinction and reflection spectra, and compared to simulated data from FDFD simulations. The optical characterization is useful to give a meaning to different phenomena occurring in our samples.

The reflection and extinction spectra of the samples were then measured while changing the polarization with an electrical stimulation. The electrical measures (current and voltage applied) were recorded and correlated in time with the evolution of the optical spectrum. A peak detection algorithm was implemented in LabView and used to detect the variation of the peak position with different polarization of the ferroelectric material.

Chapter 4

Samples production

4.1 Samples with nanodisks

The device used is described in Fig.4.1 and it is made on optic glass substrate cut in 2.5 cm square with ITO pattern deposited on it. It has two electrodes, the bottom one made of ITO and the top one made of gold. The electrodes are used to stimulate the central area, called pixel, to polarize the material. In this area, where the electrodes are superimposed, different layers are present. The first layer, above ITO, consist in an array of nanodisks, made by 3 nm titanium + 30 nm gold. The titanium layer is made for adhesion and the diameter is 160 nm. The nanodisks are dispersed on the surface, with short range order and with low nearest neighbor dispersion. The peak in nearest neighbor distance is 325 nm with a deviation of 40 nm. This value is derive in a previous work from SEM images [Shi+18].

The sample preparation is performed in a clean room class 10000 to avoid particle contamination and device failure. substrates are made by glass for microscope cut in 2.5 cm square pieces where ITO patter were previously deposited. The samples undergone to a cleaning procedure. The cleaning consist of: manual cleaning rubbing with gloves, ultrasonication with Hellmanex 2% soap for 15', rinsing with DI water for 1', ultrasonication in DI water for 15', rinsing and ultrasonicating in DI water for the second time, drying with nitrogen flow, 15 minutes UV-Ozone treatment to remove organic compounds.

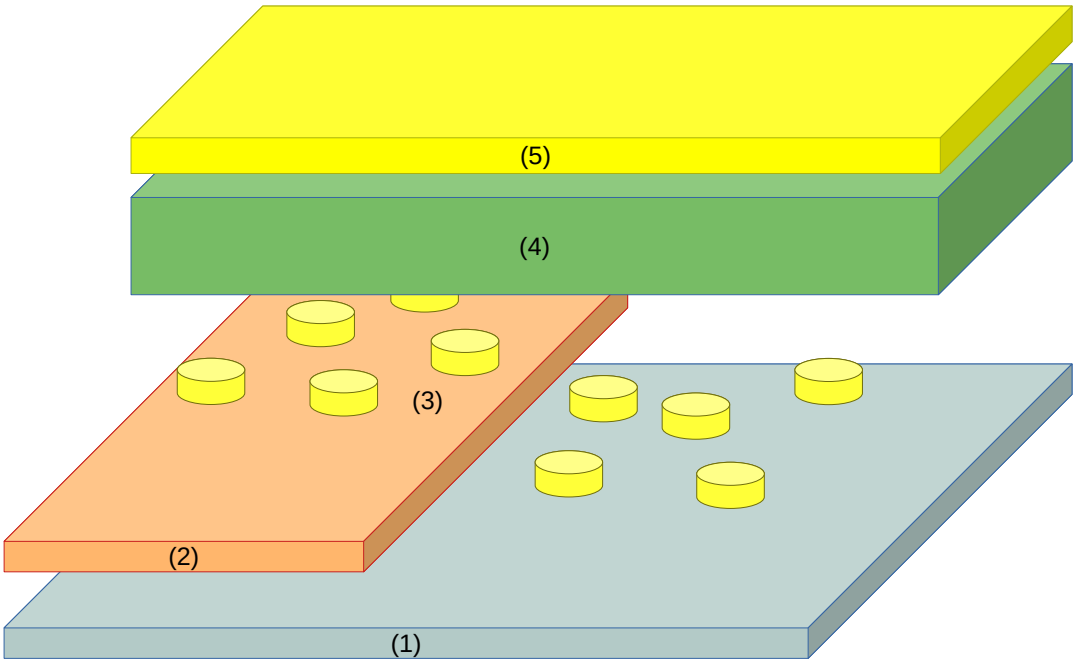

(a)

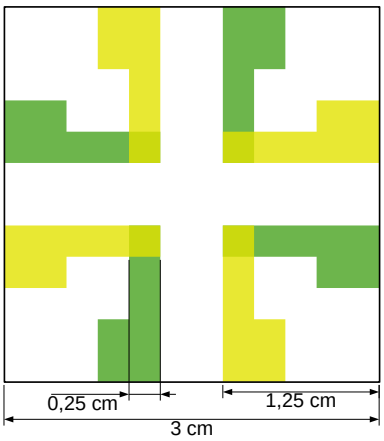

(b)

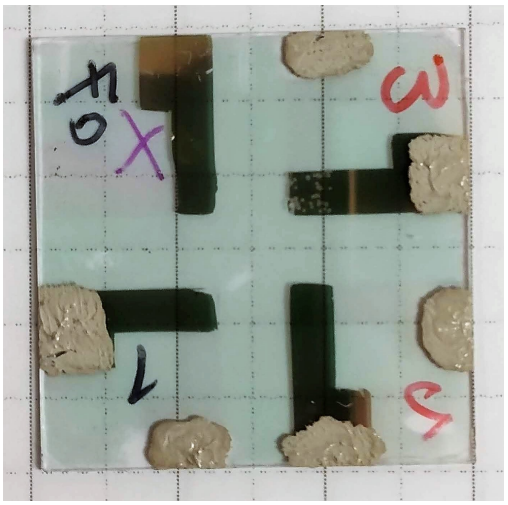

(c)

Figure 4.1: (4.1a) schematics of the device with nanodisks, not in scale: (1) Glass substrate, (2) 90 nm ITO substrate, (3) 30 nm thick gold nanodisks diameter 160 nm (4) 660 nm P(VDF-TrFE), (5) 30 nm gold electrode; (4.1b) Top-view scheme of the device with nanodisks. Four pixels with respective electrodes are shown; (4.1c) Photo showing one of the nanodisks' devices

The creation of a gold nanodisks layer is performed via a colloidal hole-mask lithography, described in the following list of processes. The steps are shown in Fig. 4.3.

1. Deposition of 140 nm sacrificial layer: a PMMA, Poly(methyl methacrylate), layer is deposited via spin coating. PMMA 4% solution in anisole is spin coated at 5000 rpm, acceleration 1500 rpm/second, time 60 s. Sample is then baked for 10 min at 170 ° C.

2. Oxigen plasma etching: sample undergo to plasma etching in the presence of oxigen, resulting in the activation of the surface through removing thin layers of material. This process improves the wettability and the adhesion on successive layers.

3. Deposition of PDDA, Poly(diallyldimethylammonium chloride) electrolyte: solution of PDDA (positively charged) electrolyte 2% in water is deposited on the samples via dropcasting. The solution is left 1 minute and then washed under DI water spill for 40 seconds. Samples are then dried with nitrogen.

4. Deposition of PS (polystyrene) nanoparticles: a water solution of PS nanoparticles 0.1% (negatively charged) is deposited on PDDA layer left for 1 minute. The sample is then gently shacked with tweezers and the residual solution washed under DI water spill for 40 seconds. Due to the opposite charges of PS nanoparticles and PDDA, the nanoparticles can stick easly to the surface creating a layer without be removed while rinsing with water. Samples are then dried with nitrogen.

5. Evaporation of hole mask layer of chromium: using "Balzers BA510" physical evaporator a chromium layer of 20 nm is deposited on the sample. The chamber with the samples inside is pumped to reach high vacuum condition. Then a metallic boat with the metal to evaporate is raised up in temperature through a current, that determines an evaporation of the material and the consequent deposition on the target.

6. Creation of mask layer: PS nanoparticles are removed via three consecutive applications of a specific tape over the chromium layer. In this way

PS nanoparticles, weakly bonded to the surface, leave holes in a layer of chromium.

7. Oxygen plasma etching: in order to remove PMMA sacrificial layer oxygen plasma etching is used as for removing photoresist in IC production

8. Evaporation of 3 nm of titanium and 30 nm of gold.

9. Lifting of of PMMA: sample is left in acetone for 30 minutes and then ultrasonicating for 30 minutes, to remove PMMA layer with the hole mask on it. Then it is washed with acetone, isopropanole and dried with nitrogen

The gold nanodisks layer is in direct contact with the ITO electrode.

A ferroelectric P(VDF-TrFE) 660 nm layer is then deposited via spin coating at 4000 rpm, 500 rpm/sec for 30 seconds. The used solution is made of P(VDF-TrFE) in diethyl carbonate 70:30 %mol. In this step is crucial to obtain a good polymerisation, so the samples are then baked in the oven for 10 minutes at 130 °C and cooled down. The procedure is repeated for three times to obtain the required thickness. This thickness is chosen large enough to avoid short circuits between top and bottom electrodes but not too high in order to allow the polarization of P(VDF-TrFE) using low voltages.

On top of PVDF a 30 nm layer of gold is then deposit by physical vapor deposition.

4.2 Samples with nanoholes

During the measurements of the optical extinction spectrum evolution while changing polarization, we noticed that the Fabry Perot cavity stretching was dominant. While applying voltage the cavity is stretched, and supports shifted modes in wavelength in comparison to no voltage applied. This effect seemed to hidden covering other possible effects to investigate. For this reason we looked for a way to avoid Fabry Perot cavity while still being able to polarize the device. We have chosen to develop an alternative device made of nanoholes on a thin film instead on nanodisks, leaving the second electrode just made of ITO, and thus transparent.

Dealing with nanoholes introduce a new physics because this structure supports the propagation of SPP and doesn't present isolated nanostructures. Anyway from the simulations we notice the plasmonic effect superimposed to the characteristic of a gold thin film. Control devices, only covered by gold thin film with no nanoholes, were created to distinguish better the nanohole plasmonic effect.

The devices with nanodisks are composed by the following layers:

- Glass substrate totally covered by 90 nm ITO layer
- 660 nm P(VDF-TrFE) layer
- 30 nm gold top electrode with nanoholes (160 nm wide)

The device schematic with quotes is shown in Fig. 4.4a. In this case we haven't used glass with ITO pattern due to the limited availability of this type of substrate.

The nanohole layer is created with the first part of the previous procedure for nanodisks (look at Fig. 4.3 steps a - d), substituting Cr with Au and Ti, leaving the mask as a top electrode structure.

In this case it is not possible to use blue tape to remove nanoparticles because it will pill off the delicate P(VDF-TrFE) layer. For this reason a water based gel with low adhesion is preferred for the process.

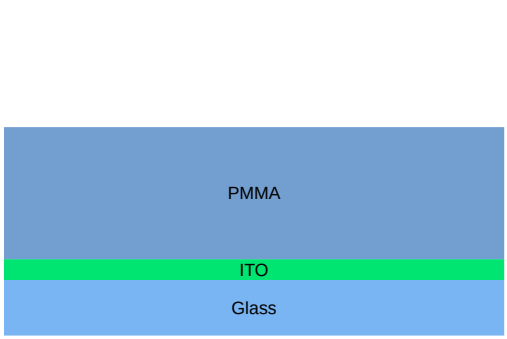
PMMA
ITO
Glass

(a)

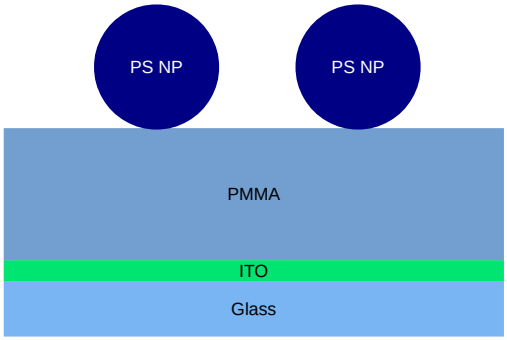
PS NP
PS NP
PMMA
ITO
Glass

(b)

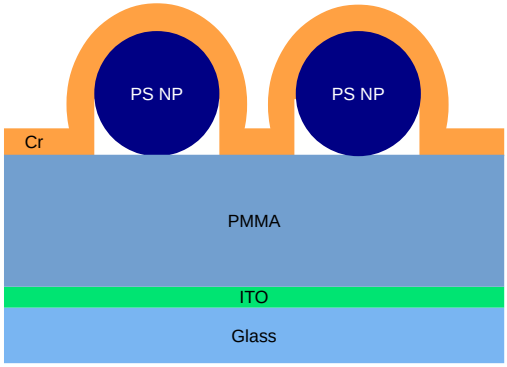
PS NP
PS NP
Cr
PMMA
ITO
Glass

(c)

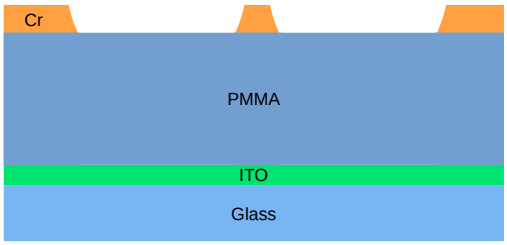
Cr
PMMA
ITO
Glass

(d)

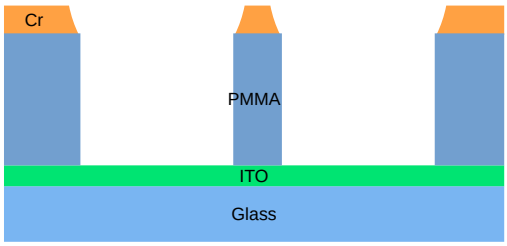
Cr
PMMA
ITO
Glass

(e)

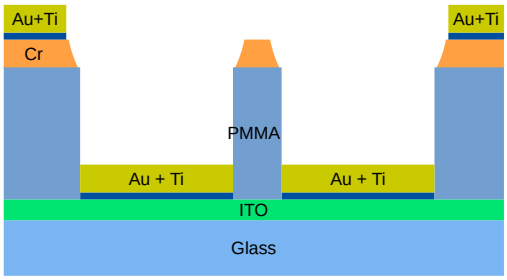
Au+Ti
Au+Ti
Cr
PMMA
Au + Ti
Au + Ti
ITO
Glass

(f)

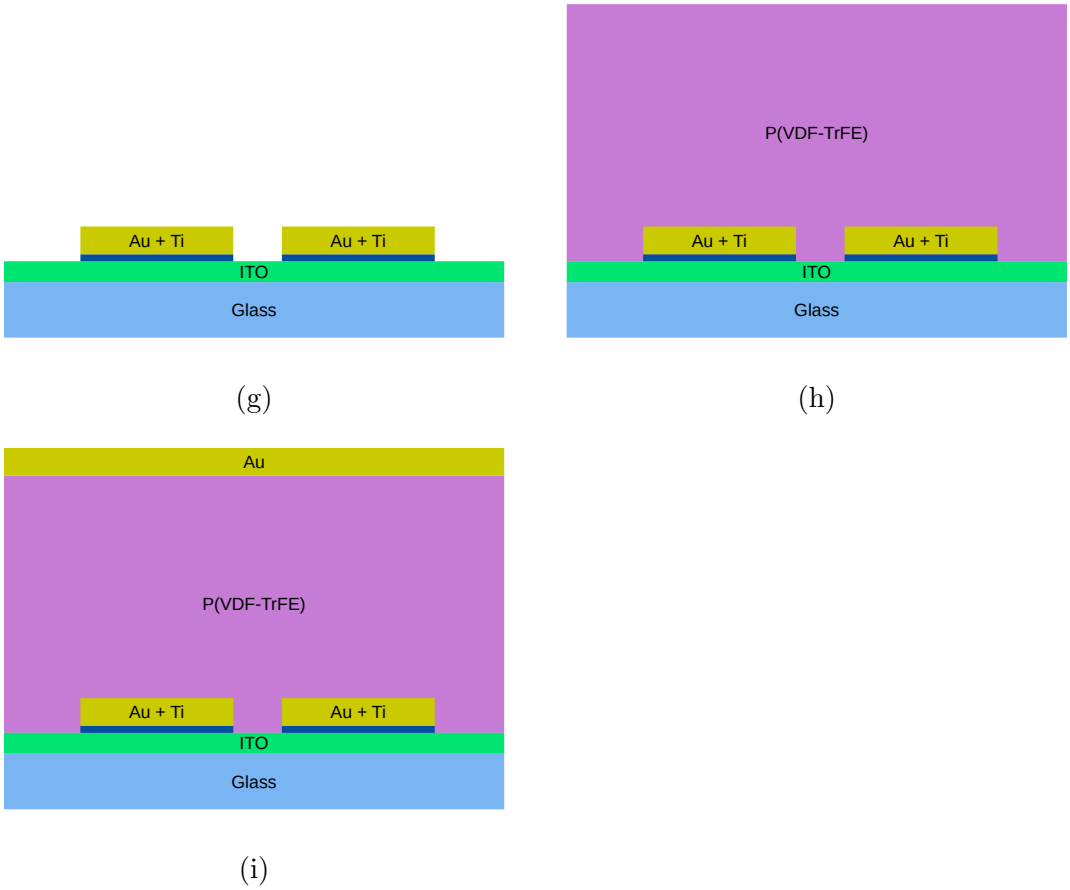

Figure 4.3: Procedure to create hybrid plasmonic-ferroelectric devices with nanodisks. The device is shown in section from the side. (a) PMMA layer is deposit by spin coating. (b) Electrolyte and PS nanoparticle (diameter 158nm) in water solution are deposited on the substrate. (c) Chromium layer is evaporated by PVD. (d) nanoparticles are removed by sticking blue tape and removing it. (e) PMMA layer is etched with oxygen plasma etching. (f) Titanium adhesion layer and gold layer are deposited. (g) sacrificial mask layer is removed ultrasonicating in acetone. (h) different layers of P(VFD-TrFE) are spin coated on the substrate to reach the right thickness. (i) gold top electrode is deposited by PVD.

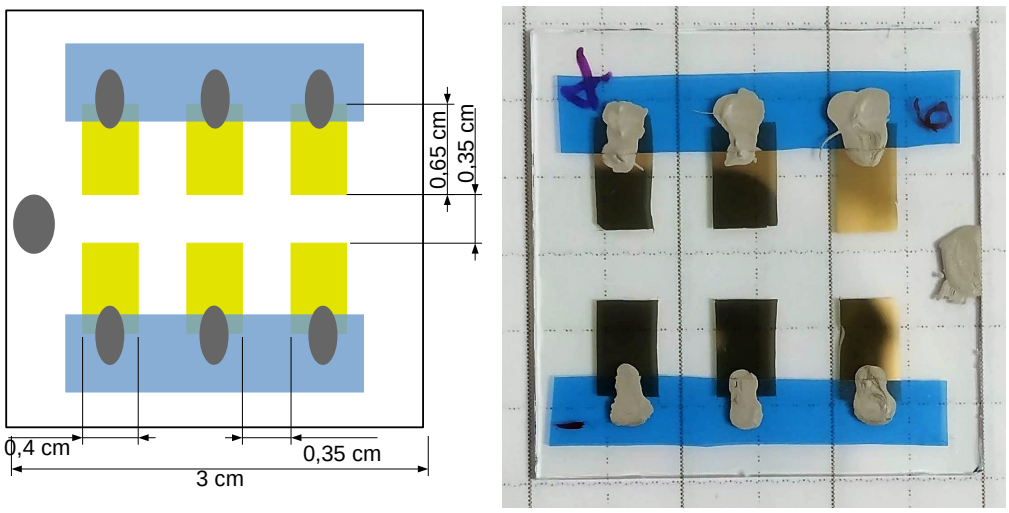

(a) (b)

Figure 4.4: 4.4a This schematic describes the structure and the dimensions of the devices with nanoholes. The bottom layer is glass covered with ITO. On this layer a P(VDF-TrFE) film divides the bottom electrode with the top electrode (yellow rectangles), composed by 30 nm gold film with nanoholes. The adopted geometry of top electrode avoid accidental faults by short circuit because gold top electrode is not covering the edge of substrate, where P(VDF-TrFE) is less uniform. To contact electrically the device, a piece of protective blue tape (blue rectangles) is attached and overlaps the electrodes. A spot of silver conductive paste (grey ellipse) create a solid connection for top electrode. Another spot of silver paste, in an area where P(VDF-TrFE) is removed, create the bottom electrode connection. 4.4b Picture of a used device.

Chapter 5

Optical and electrical measurements

5.1 Optical setup and instrumentation

The optical characterization of the devices is performed using Andor Shamrock 303i spectrometer, coupled with an Andor Newton 970 EMCCD camera, both controlled and acquired via PC. Andor newton camera is connected to PC via USB cable and the Shamrock spectrograph is connected to the camera via I^2C cable. The Spectrograph contains EEPROM containing calibration info written during calibration procedure. The light sources used are a stabilized xenon lamp and a microscope incandescent light used for transmission measurements.

Despite the xenon lamp shine more stable light, it present some very strong emission lines in near infrared, that in many cases coincide with the region of interest. The microscope transmission light is preferred, showing a more broad and uniform spectra in the near infrared region.

Using microscope setup, the samples are directly placed on the microscopic plate and the microscope is focused on one pixel using the lowest magnification (10x) to collect as much transmitted light as possible, to increase the signal to noise ratio and improve the final results. The optical fiber is coupled to the top mount of the microscope and it receives a fraction of the collected light. The fiber is then coupled to the spectrometer. The setup is described in the diagram of Fig.

5.1.

5.2 Electrical setup and instrumentation

To polarize the ferroelectric material it is necessary to provide a voltage between two electrodes.

Because of the high probability of failures during the production procedure it is necessary to have a feedback about the performance of the device in terms of polarization. The current absorbed by the device after setting a high enough voltage is a good indicator of a successful polarization. Usually the currents' value starts from an initial value of $10^{-6}A$ and decreases asymptotically to $10^{-9}A$.

For the voltage stimulation and the current measurements we use Keithley 2400 source-meter. This instrument is controlled via software and can read data in non - buffered mode with sampling time of 50 ms.

The sample is connected to the Keythley by a piece of copper wire that is attached to the bottom of a small glass substrate (2.5 x 4 cm) with tape and is gently left touching the electrode. In this way we avoid damages to the thin electrode.

5.3 Data acquisition

Spectra are acquired from Andor spectrometer using the specific Andor Solis software. We used that program to acquire single spectra.

To monitor the evolution of the spectra while changing the polarization of the material it is necessary to perform a long acquisition (2' for each step) in order to avoid transient phenomena. We repeat the measurement for several times to have good statistics on the data. At the same time is necessary to control the applied voltage from the Keithley source-meter and to monitor the current.

Although the Andor Solis software allows fine tuning of all the parameters of the camera, it is not designed to acquire long series of spectra, then the acquisition is performed through a custom LabView program that I developed using Andor Software Development Kit (SDK) libraries. The specifications of this program in-

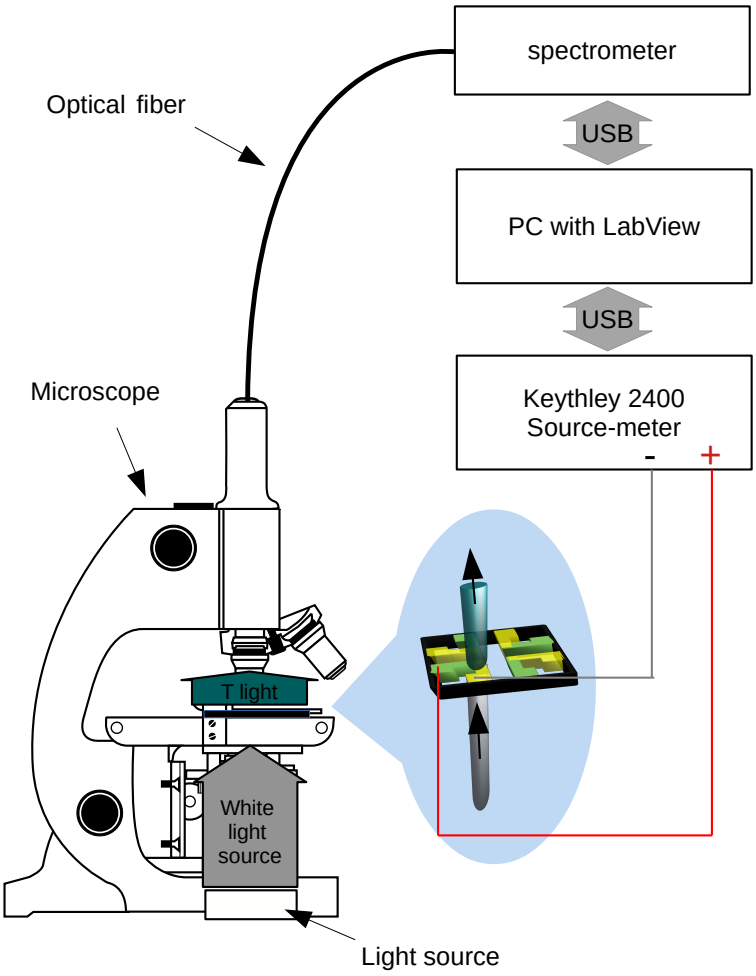

Figure 5.1: Experimental setup schematics. The sample is placed on the microscope plate and the light for transmission measurements is illuminating the sample from the bottom (nanodisks layer). The microscope is focused on the pixel area and the collected light is transferred to the spectrometer via an optical fiber. The Keithley source-meter is stimulating electrically the sample, allowing changes in polarization. The Keithley cables are gently connected to the sample via two connectors that we made. The connectors consist in one piece of copper wire attached on the bottom of a piece of glass. The glass weight let the wire staying attached without compromising the thin electrode.

clude fast continuous acquisition from Newton camera, efficient background and reference treatment, tuning of spectrograph parameters (like grating, slits apertures, etc.). A schematic of the program is shown in Fig. 5.2.

The acquisition part of the program consists in three different separate programs (see Fig.5.2). The first one controls the parameters of the Shamrock spectrograph, the second one controls the camera of the Andor spectrometer and the third controls the Keithley source-meter.

5.3.1 DAQ from Shamrock spectrometer

The first program to run is "Sub-VI Shamrock". The program control the parameters of the spectrograph like the slit aperture, the used grating, the central wavelength for measurements and other settings.

While initializing the instrument, the program reads EEPROM information and save it in a global variable, used by the acquisition program. This allows to match acquired data with minimum and maximum wavelength of the spectrum, giving to each pixel the related wavelength.

When a parameter is changed in spectrograph setup, the program is calling the specific function to perform the required action, then the modified EEPROM info are updated.

5.3.2 DAQ from Andor Newton camera

The program to acquire spectra from Newton camera is based on a queued producer-consumer state machine (Fig. 5.2). The interface (Fig.5.3) allows the user to perform different actions: set the sensor temperature (from room T to -60°), define reference and background spectra, start and stop the acquisition, choose where and how to save data, compute and show peak position and spectra while measuring, choose plotting on screen frequency, choose smoothing for acquired data, choose if to acquire averaged spectrum or single spectrum.

Looking at the code, for each action in the front panel the producer-loop is enqueueing one element with the relative label. The consumer loop is normally idle. When one element is enqueued, the loop remand to the specific case to

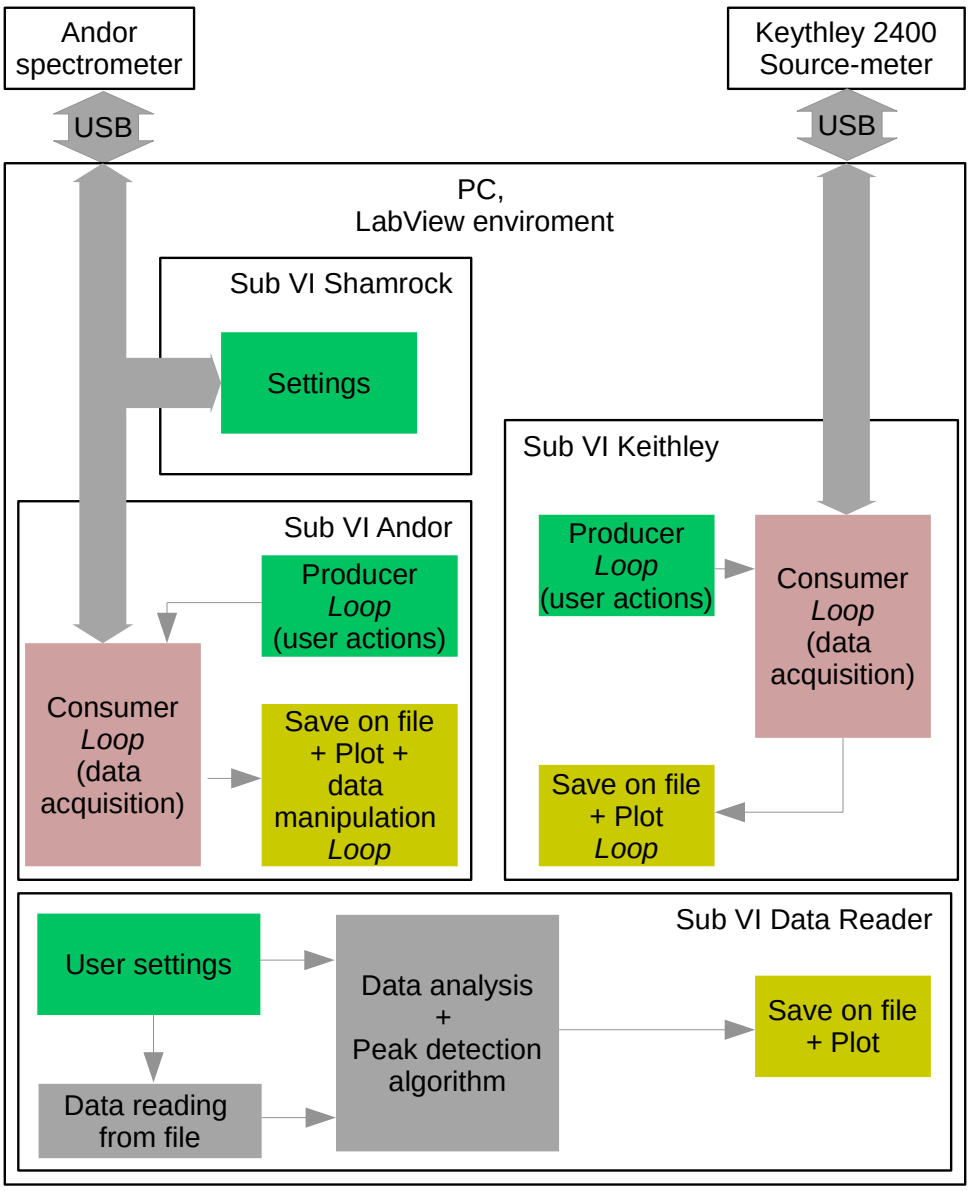

Figure 5.2: Schematics of the program for data acquisition and data analysis. The program can interface with the instrumentation to set the acquisition mode. In each data acquisition Sub-VI: a producer loop based on event structures reacts to the user action and queues the instructions, a consumer loop performs the acquisition with specific timing and the saving loop plots the data on screen and saves data into files. Shamrock Sub-VI reads and sets parameter for the spectrograph. The data reader sub-VI is used after the data is acquired. It analyzes the acquire data, finds the peak position evolution in time, and saves the results.

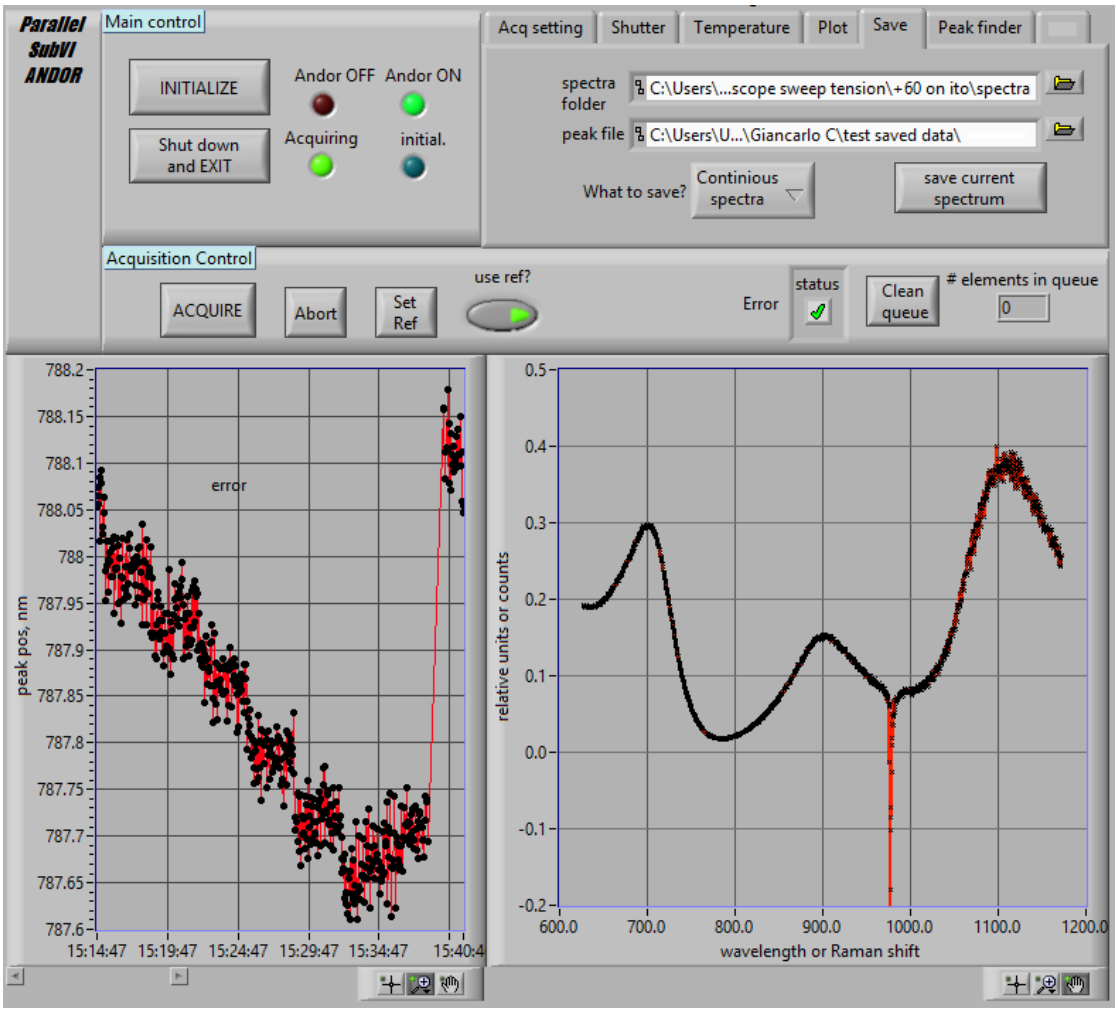

Figure 5.3: Interface of "SubVI Andor", used to acquire data from the spectrometer. Main control panel is used to initialize and shout down the instrument. Acquisition control is used to start and stop the acquisition. When the system is idle it is possible to set reference and background by "Set ref" button, which opens a separate window. "Clean queue" button is used to cancel the piled up commands in case of errors. The tabular control let users access to the settings: "Acq setting" changes acquisition mode and selects sampling frequency, "Shutter" opens the internal shutter, "Temperature" sets T from room temperature to -60°, "Plot" sets which plot to show and the refreshing frequency, "Save" sets saving paths and the mode of saving, "Peak Finder" sets the parameters to compute the algorithm for peak detection.

perform the action. While the action is performed, the user loop is still capable to respond to front panel action, avoiding unresponsive behaviour.

Since data saving and plotting slow down the program if done for each instrumentation call, data is enqueued in a buffer. Only after a certain settable time a parallel loop takes this buffer of data and processes it. During this operation, depending on the mode selected, the program computes the peak via centroid method, saves the value or saves directly all the spectra in different files. Using this technique we reached a delay time of 10 ms between acquisitions. The sampling frequency is then mainly limited by the exposure time of the camera.

The raw data acquired from the camera is an array of 1600 values from 0 to 65535 (16 bit) depending on the light intensity on the particular horizontal position in the sensor. The acquisition mode is full vertical binning, for which the pixels values in one column of the sensor are averaged.

The program can save raw data or transmittance (ratio). For the latter it is necessary to acquire the reference spectrum and the background. The reference spectra for transmission measurements is the source light without any filter, while for reflectivity measurements is the reflected source light by a mirror.

The transmission is computed as in Eq. 5.1, where S is the acquired signal, B the background, R the reference. To maximize the signal to noise ratio of the final signal, R and B spectra are acquire separately before starting the acquisition, averaging many spectra. An improvement is noticed averaging at least 20 spectra.

$$T = \frac{S - B}{R - B} \tag{5.1}$$

All the saved data have time reference, in order to correlate them with measurements from other instruments. A complete time - string is collected when data is read from spectrometer.

5.3.3 DAQ from Keithley Source-Meter

For polarizing the ferroelectric material Keithley 2400 Source-meter is used.

The program (see Fig. 5.2) is based on producer consumer loops, the same structure described in the previous chapter. The program, when the instrument is initialized, can set different voltages for a defined period of time. User set the time

delay between points. For each point we ask the instrument to output a specific voltage and measure the current. The supported modes for voltage output are:

- Sweep: the user sets minimum voltage, maximum voltage, steps. The program does a sweep from minimum to maximum voltage, with the possibility to descend the ramp
- Step sweep: this mode acts like the previous one, but for each step a defined number of points are recorded.
- List: user sets a list of voltages with related number of points to record

A parallel loop collects the acquired data and append it to a file selected by the user. This file contains three columns: time reference (string), voltage, current.

5.4 Data processing and peak detection

For this study it is necessary to distinguish the effect, on our hybrid devices, of different polarization of the ferroelectric material. The effects that we are investigating, like LSPR and Fabry-Perot cavity, can be studied looking at the optical response variation. Each effect is associated to a spectra profile presenting peaks in transmission, extinction or reflection. It is necessary to find a method that allows to determine the peak position with the minimum error.

The transmission spectra presents a profile with peaks that are not suitable to be fit by standard peak functions. This happens because the spectra is the result of the overlap of different effects such as Fabry Perot cavity effect, plasmonic resonance effect, and transmission of metal thin-films.

For this reason a different approach, called centroid method, is used. The method were evaluated by Dhalin et al. in comparison to other peak detection methods, showing lower noise in the peak position signal [DTH06].

Given a specific function and an interval, the centroid in x (wavelength) coordinate is calculated from Eq. 5.2. The technique fits a function on the spectrum portion close to the peak, then computes the centroid. In our case we fit a polynomial with coefficients p_i and the centroid position and the peak value is written as Eq. 5.3.

In the case of a polynomial fit it is easy to compute the integral and use this for a quantized wavelength spectrum, Eq. 5.4.

$$\lambda_c = \frac{\int_{\lambda_a}^{\lambda_b} \lambda(E(\lambda) - E(\lambda_a))d\lambda}{\int_{\lambda_a}^{\lambda_b} E(\lambda) - E(\lambda_a)d\lambda} \tag{5.2}$$

$$\lambda_c = \frac{\int_{\lambda_a}^{\lambda_b} \lambda \sum_{i=0}^{n}(p_i\lambda^i - p_i\lambda_a^i)d\lambda}{\int_{\lambda_a}^{\lambda_b} \sum_{i=0}^{n}(p_i\lambda^i - p_i\lambda_a^i)d\lambda} \tag{5.3}$$

$$\lambda_c = \frac{\sum_{i=0}^{n}[\frac{p_i}{i+2}(\lambda_b^{i+2} - \lambda_a^{i+2}) - \frac{p_i}{2}\lambda_a^i(\lambda_b^2 - \lambda_a^2)]}{\sum_{i=0}^{n}[\frac{p_i}{i+1}(\lambda_b^{i+1} - \lambda_a^{i+1}) - p_i\lambda_a^i(\lambda_b - \lambda_a)]} \tag{5.4}$$

The algorithm to calculate the centroid proceed as follows. The input is a spectra and the input parameters are the estimated peak position, the peak span, the polynomial order to perform the fit and the range of data to compute. Initially the spectra is restricted to the selected range, then the wavelength is transposed linearly into a new relative coordinate, to make the computation of the fit more simple. After that the fit is performed, resulting in an array of coefficients. The polynomial function in $\lambda_a = c - s$ (c estimated center, s width of the peak) is then subtracted to the polynomial, and the next zero of the function is then found, called λ_b.

Using λ_a and λ_b as boundary it is possible to compute peak position from Eq. 5.4.

I used a polynomial order $n = 10$. Higher polynomial order doesn't show significant improvement and create more noise in the peak position.

The algorithm is developed in a LabView program called SubVI Data analysis (see Fig. 5.2). This program works as following:

- User select the spectra files that are named with a time string relative to the acquisition time.
- User select electrical measurements file, containing time string, voltage value, current value
- User sets the parameters for the peak detection algorithm: estimated peak position, peak span, spectra portion to consider.

- The program computes the peak position for each spectra in input.
- Each peak position is correlated to a time string that is reconstructed from the file name.
- Current and voltages are extracted from the relative file and associated to the relative time constants.
- Peak position, current and voltage values are plotted in a multi-graph that allows x scale in time- reference constant (LabView have a specific format which includes date and time with 1 ms precision).
- This three values are saved in new files, one for peak position and one for current and voltage. The time reference is in seconds. The zero for this reference is set for the first acquired spectra and relate to the currents/voltages times.

5.5 FDFD simulations

Finite difference frequency domain (FDFD) simulation are used to better explain the experimental acquired spectra. The simulations are performed with Comsol 5.1 treating the problem as a propagation of monochromatic waves in sub-wavelength structures. This method finds an approximate solution for the frequency domain form of Maxwell equations into the structure, that is divided into different regions, forming the mesh of the model. In our case the mesh was tetrahedral. The maximum element size, for each material, is choosed to be $\lambda/n/M$ where $M = 7$ is the mesh factor, n and λ respectively the refractive index of the material and the minimum simulated wavelength.

The model used is composed by different domains (see Fig. 5.4) where, on the faces normal to x and y axes, periodic boundary conditions are set to simulate an array of nanodisks or nanoholes. The approximation of periodic structure is acceptable because nanodisks, with the obtained periodicity, doesn't show collective effect. Changing the spacing the simulated spectra doesn't differ and using scattering conditions the results are not coherent with observed spectra.

The field profile shows significant field enhancement only in a small region close to the nanodisks.

On both the top and the bottom of the structure there are two regions (called "ports") where Comsol probes the field. The input port is set to generate a specific wave vector with a defined polarization, while the output port is a perfect scatterer for incident radiation and measures the output power. The input port is placed under the glass layer while the output port is placed over the air layer. By performing the ratio of output and input power I find the transmission spectra for a wavelength. The input port also measures the incoming reflected radiation, allowing to obtain reflected spectrum.

The wavelength dependent refractive indexes for common materials are found from a database online based on literature [19] while the refractive index for P(VDF-TrFE) is found in literature [Wan+06] and is 1.42 with a small dependence on wavelength.

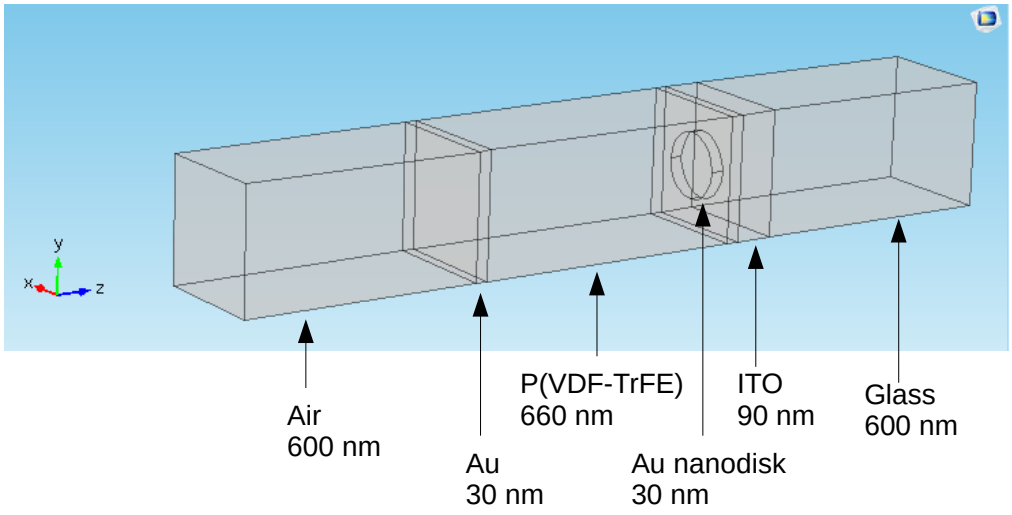

Figure 5.4: Geometrical structure of the simulated model. The Au nanodisk is coupled to P(VDF-TrFE) The input port is on the right side of the structure, perpendicular to z axis, while the output port is on the left side of the device. The long air and glass sections avoid interferencial effects and imitate measurements in the far field.

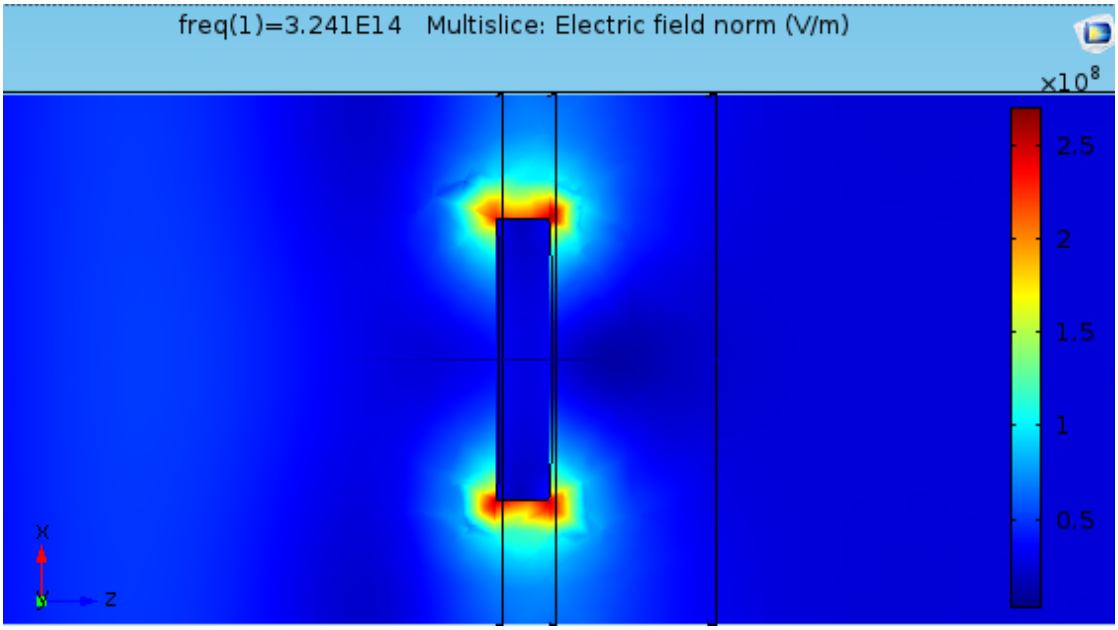

Figure 5.5: Field profile for a simulation at λ=900 nm with nanodisks samples. The field profile in correspondence to the nanodisk doesn't show significant changes for different wavelengths. The field enhancement near to the surface of the nanodisk is compatible with a presence of a localized LSPR . The system input is unitary H field in y coordinate

Part IV

Results

In the first chapter the results of the sample production are reported. Then in the next chapter the results of optical characterization are shown. We distinguish between different observable effects.

The samples are then electrically stimulated through different type of signals. The peak position, for various peaks of the spectra, is correlated with the applied voltage and the polarization state of the ferroelectric material.

5.6 Sample production

The produced samples are composed by a ferroelectric layer coupled to an array of gold nanodisks showing LSPR. The whole device is enclosed between two electrodes, that are used to polarize the ferroelectric layer.

During sample production many steps were critical to achieve good results. The main problem encountered was the fault of the middle P(VDF-TrFE) layer, with consequent short circuit of the sample. This problem was solved by performing the production in the cleanest conditions, because deposited dust particles can result in lack of uniformity for the ferroelectric layer. Holes are left by removed dust, that can let evaporated gold to be in direct contact with the conductive substrate under P(VDF-TrFE).

Another problem was the uniformity of P(VDF-TrFE) layer, caused by a wrong spin coating procedure. In this case adding more solution before spin coating solved the problem. Many devices resulted fault, thus identical devices from a previous project [Shi+18] were used in some cases.

During the optical measurements we noticed that the samples show a pronounced Fabry Perot cavity effect that is dominant in comparison to plasmonic effect. To make it less pronounced we decided to produce samples with one electrode made on ITO and one with gold layer with array of nanoholes. In this case the physical phenomena is different than for nanodisks array, but it still shows an extinction peak due to plasmonic effects.

For samples with nanoholes the top electrode have an influence on the probability of short circuits. Due to a limited availability of patterned substrate, the samples with nanoholes were produced on fully ITO-covered substrates. Initially the top electrode was kept as for nanodisks substrate (with branches , Fig. 4.1b

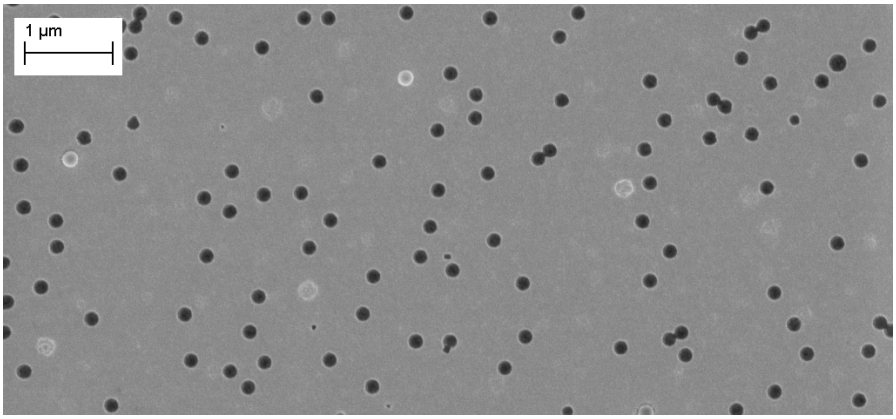

(a) SEM image of nanoholes in 30 nm gold film. The distribution differs from short range order due to high dispersion

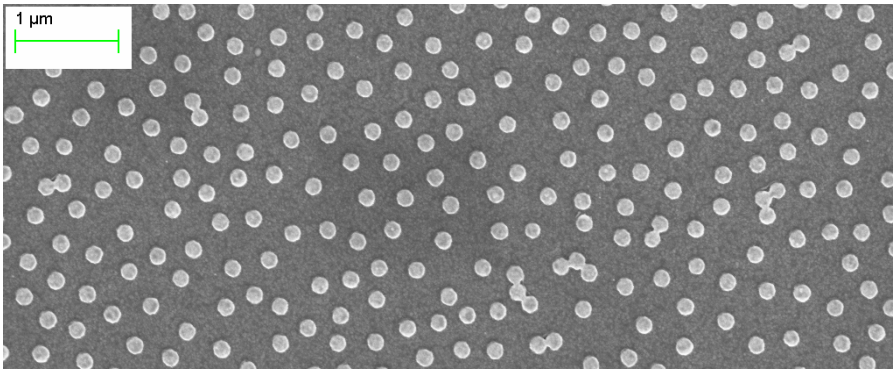

(b) The distribution of gold nanoparticles on ITO shows short range order. The peak in nearest neighbor distance distribution is 325 nm, with std deviation of 40 nm as measured in previous works [Shi+18]

Figure 5.6

reaching the border of the device). In this case all the devices got short circuited, probably due to the lack of uniformity of spin coated P(VDF-TrFE) close to the edge of the substrate. From this geometry we moved to rectangular electrodes in the center of the device.

Devices with gold nanodisks show a better and more uniform distribution in comparison to the distribution of nanoholes in the other type of devices (Fig. 5.6) . The difference in distribution can be caused by the different hydrophilicity of the substrate. During the deposition of nanoparticles, indeed, the solution was hard to spread on the whole surface in the case of P(VDF-TrFE) covered substrate. On oxygen-plasma treated ITO, instead, the solutions with electrolyte PS nanoparticles spread more easily and require less amount of solution to cover the whole surface.

5.7 Optical spectra

Devices extinction spectra were optically characterized (see Fig. 5.7i).

Looking at the spectra of the nanodisks device with the gold layer on top (Fig. 5.7i curve a) peaks at 625 nm, 780 nm and at 980 nm are visible. Wells are present at 525 nm, 700 nm and 900 nm. This spectra results from a combination of LSPR effect and Fabry-Perot cavity effect.

Comparison with device with no nanodisks

It is interesting to relate the extinction spectra of the device (Fig. 5.7i curve a) with the extinction spectra of a similar device with no nanodisks (Fig. 5.7i curve b). We can see that at 700 nm the first presents a well in extinction due to a resonant mode in the cavity.

Comparing the peaks in extinction at 780 nm, for the full device (Fig. 5.7i curve a) the extinction is higher than for only the top electrode gold film (Fig. 5.7i curve b). For other peaks in extinction, for example at 625, the value for the device (Fig. 5.7i curve a) and for a gold film (Fig. 5.7i curve b) is the same. This is an evidence that a different effect is absorbing or reflecting light. A possible explanation for this effect is LSPR.

Comparison with device with only nanodisks

If we consider spectra acquired from devices without the top electrode, is possible to notice the plasmonic extinction peak around 750 nm and 776 nm for nanodisks covered by P(VDF-TrFE) on, respectively, glass (Fig. 5.7i curve c) and ITO (Fig. 5.7i curve d). The peaks are shifted because of the different refractive index of the nanodisks surrounding, giving a shift in the LSPR extinction peak.

Resonant modes of a similar Fabry Perot cavity

The resonator modes can be calculated from the dimension of the cavity $d =$ 660nm and the refractive index of P(VDF-TrFE) $n = 1.42$ [Wan+06] and are listed in Tab.5.1.

On the resonant wavelengths the Fabry Perot cavity allows maximum trasmittivity and minimum extinction, but we can observe that in (Fig. 5.7i curve a) for 626 nm peak the spectrum presents a peak in extinction. A possible explanation is that the mirror composed by nanodisks array give a phase shift to the reflected light, modifying the resonant condition.

Mode	Wavelength (nm)
1	1878
2	939
3	626
4	469

Table 5.1: Modes of the Fabry Perot cavity between gold nanodisks and gold film

Comparison with simulated data

It is also possible to compare acquired spectra of Fig. 5.7i with simulated data of Fig. 5.7ii. Comparing the measured spectra of the device (Fig. 5.7i curve a) with the simulation (Fig. 5.7ii curve f) it is possible to see that the position of the peaks are compatible with the experimental data. Simulated spectra shows more sharp peaks while measured are more broad and the position is not exactly the same. The broadening is caused by the non periodicity of the real nanodisks distribution and the shift in position by the non uniformity of the P(VDF-TrFE) layer. This shifts can cause differences in the thickness and then in the modes of the cavity. By averaging over the different thickness cavity modes the result is a broadening of the Fabry Perot peaks.

Comparison between simulated devices with nanodisks and simulated devices with double gold thin film

Comparing instead the two simulated curves for full devices (Fig. 5.7ii curve f) and devices with only two gold reflective layers (Fig. 5.7ii curve e) we expect a sharpening of Fabry Perot peaks, due to the enhancement in reflectivity with the double reflective layer. The peak at 700 nm of (Fig. 5.7ii curve e) is indeed more sharp but the peak at 900 nm disappears, this can be related to the phase shift of the plasmonic surface, that modifies the resonance condition and moves the peak.

The difference between (Fig. 5.7ii curve f) and (Fig. 5.7ii curve e) can not be related to a plasmonic effect because, in the simulation, the surrounding material of the nanodisks is the same for the two curves, so the resonance is not changed.

Comparison with measured spectra in reflectivity

The samples have been tested also in reflectivity because the FP cavity shows high extinction in the region where also the plasmonic effect is present, suppressing its final contribution to the spectrum.

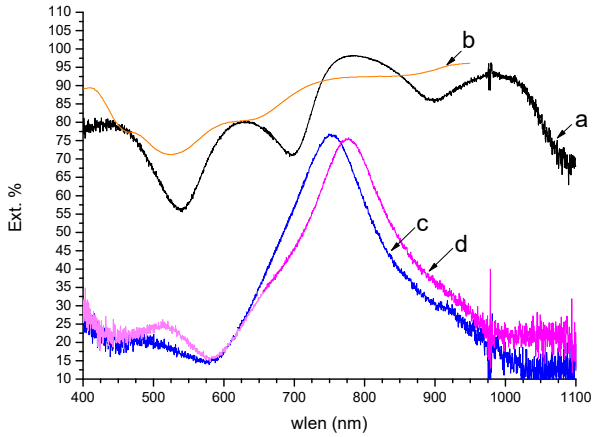

(i) Measured extinction spectra of different type of devices with nanodisks: (a) Full device with, layered, glass, ITO, gold nanodisks, P(VDF-TrFE) layer, gold top electrode layer, as discussed in experimental section, (b) Device composed by layers of glass, ITO, P(VDF-TrFE), gold top electrode, (c) Device composed by glass, gold nanodisks, P(VDF-TrFE), (d) Device composed by glass, ITO, gold nanodisks, P(VDF-TrFE).

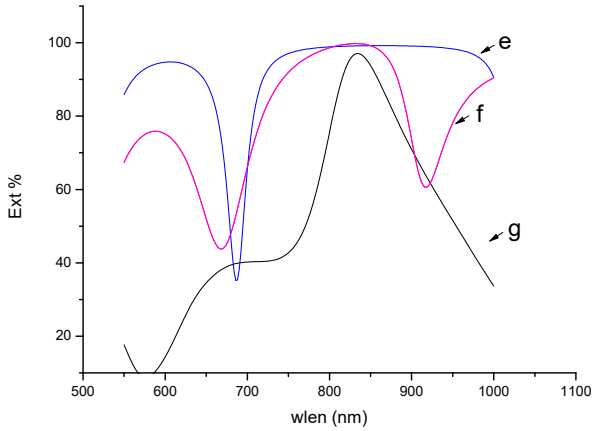

(ii) Simulated extinction spectra: (e) Device composed by layers of glass, Au, P(VDF-TrFE), gold top electrode, (f) Full device with, layered, glass, ITO, gold nanodisks, P(VDF-TrFE) layer, gold top electrode layer, as discussed in experimental section, (g) Device composed by glass, ITO, gold nanodisks, P(VDF-TrFE).

Figure 5.7: Measured and simulated extinction spectra for devices with nanodisks

Looking at the measured spectra for full devices with nanodisks we notice that the peak at 780 nm in extinction (Fig. 5.7i curve a) corresponds to a peak in reflection at the same wavelength (Fig. 5.8i curve h). This tells that a low amount of light is absorbed by the device.

The response for devices with only nanodisks without top electrodes is different because the transmission at the peak at 750 nm of (Fig. 5.7i curve d) differs from (Fig. 5.8i curve i) by 35%. This indicates an absorption by the nanodisks without top electrode and Fabry Perot cavity effect.

Comparison with simulated spectra in reflectivity

Looking to the simulated spectra of device with nanodisks (Fig.5.8ii curve m) it is possible to notice that, compared with measured data (Fig. 5.8i curve h) , the peaks are not correspondent and seem shifted (reflection well at 675 nm for simulations and 700 nm for measurements)

Looking at the simulated extinction response of the device without gold top electrode (Fig. 5.7ii curve g), the peak in extinction at 850 nm corresponds to lower reflection. The absorbed light is on the order of 25%, lower than in the measured case. At the same time the simulations shows that a low portion of incident light is absorbed at 920 nm.

5.7.1 Samples with Nanoholes

The samples with nanoholes were realized to avoid the FP cavity stretching effect leaving visible only the plasmonic effect.

Once measured the sample in extinction (Fig. 5.9 curve q) , and compared with control samples with no nanoholes on top (homogeneous gold film) (Fig. 5.9 curve p) it was evident that the plasmonic effect was not strong, because the distribution of the nanoholes show higher dispersion (Fig. 5.6a) .

Comparison with simulations

Three simulations have been performed to understand better the spectra observed. In this simulation the periodicity of the nanoholes are different: 0.3 μm, 0.35 μm, 0.4 μm. Larger spacing requires too large computational capabilities that were not available. Anyway the three extinction spectra show that plasmonic well is red shifted increasing periodicity, that can explain the small well appearing

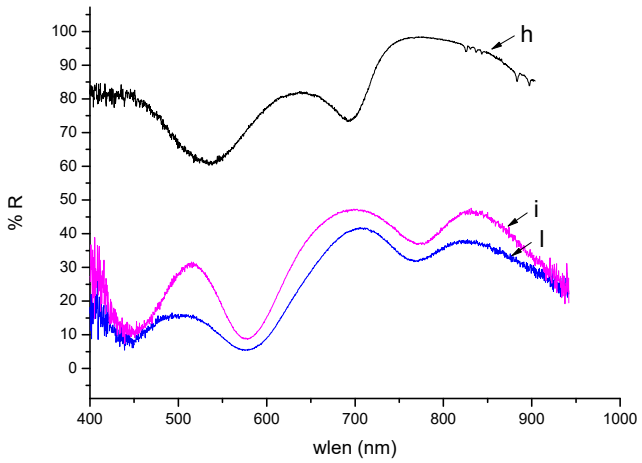

(i) Measured reflection spectra: (h) Full device composed by glass, ITO, nanodisks, P(VDF-TrFE), gold top electrode, (i) reflectance of, layered, glass, ITO, P(VDF-TrFE) layer, gold top electrode layer. (l) reflectance of, layered, glass, nanodisks, P(VDF-TrFE) layer

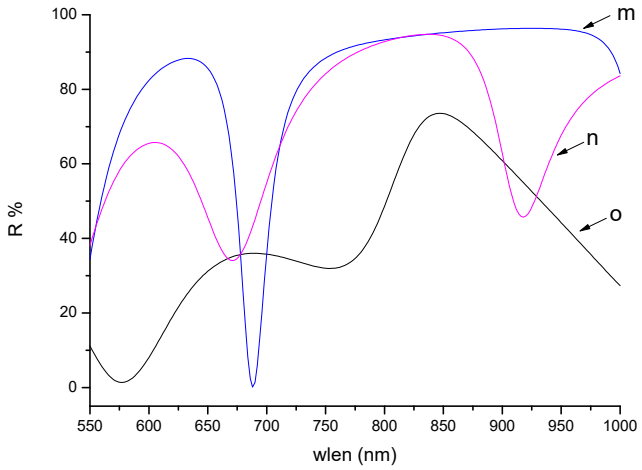

(ii) Simulated reflection spectra: (m) Device composed by layers of glass, Au, P(VDF-TrFE), gold top electrode, (n) Full device with, layered, glass, ITO, gold nanodisks, P(VDF-TrFE) layer, gold top electrode layer, as discussed in experimental section, (l) Device composed by glass, ITO, gold nanodisks, P(VDF-TrFE).

Figure 5.8: Measured and simulated reflection spectra for devices with nanodisks

at 860 nm comparing the control spectra (Fig. 5.9 curve p) and the full device spectra (Fig. 5.9 curve q). In this case the plasmonic effect is superimposed to the characteristic extinction of a gold film.

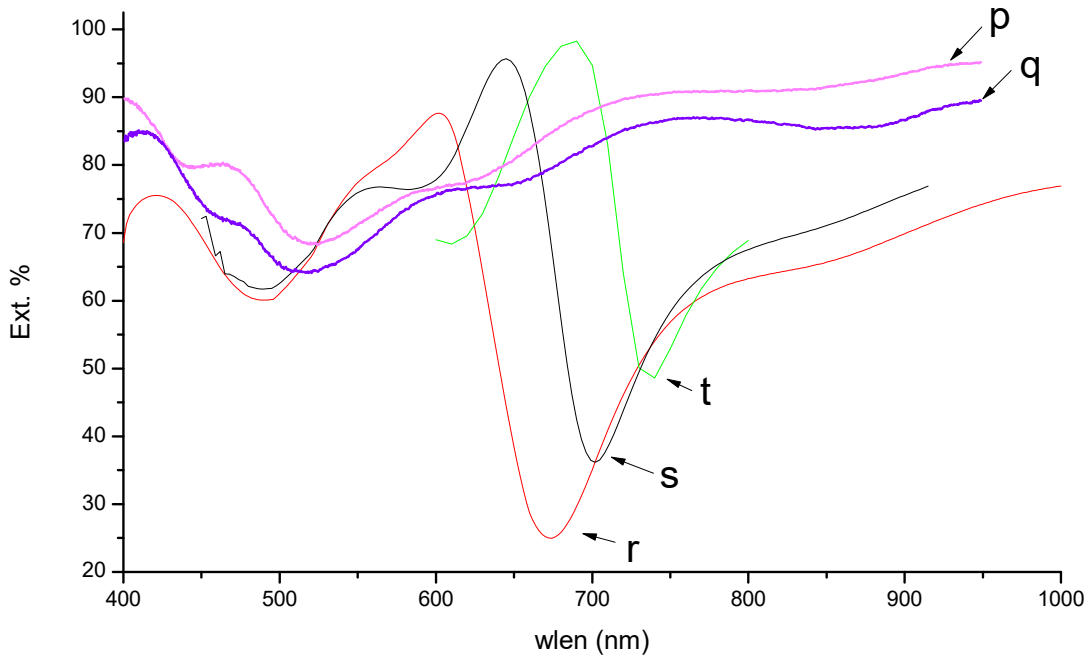

Figure 5.9: Different extinction spectra for samples with nanoholes: (p) control sample with layers of ITO, P(VDF-TrFE), gold. (q) sample with ITO, P(VDF-TrFE), gold layer with nanoholes. (r, s, t) simulated spectra for periodic structure with layers of ITO, P(VDF-TrFE), gold nanoholes. The periodicity is respectively 0.3, 0.35, 0.4 μm. To notice that the well give by the plasmonic resonance is moving close to the observed peak and the minimum value in the well is getting higher, as in measured data.

5.8 Optical effects due to electrical stimulation

5.8.1 Electrical poling process

To reach the polarized state and invert the polarization of the ferroelectric layer it is necessary to make the P(VDF-TrFE) uniform with all the polarization domains oriented in the same direction.

The devices were electrically stimulated in different ways.

First step was the poling process. This process consists in applying alternatively, for many cycles, a sweep in voltage with $V_{max} = 60V$. During this process the randomly oriented polar domains, given by the orientation of P(VDF-TrFE) molecules, switch from chaotic to oriented. During this cycles the electrical response of the device was very unstable, showing unpredictable current spikes for different voltages.

After few cycles (four) the response of the device becomes more predictable, showing a spike in current around $V_{th} = 30V$, depending on the device, that is the limit threshold voltage to switch permanently the polarization of the dipoles. The maximum applied voltage is 80V, depending on the device. With higher voltage the breakdown value is reached and the device get shorted. This initial step was performed in all the devices in order to obtain a better results.

Fig. 5.10 shows voltage-current curves acquired from five different samples and the result is reproducible. In many produced samples (Fig. 4.4b) there have been faults after some cycles of poling. The electrical response, during the bias of the samples, shown very low resistance , related to a short circuit of the device. The possible cause of this effect can be related to a damage of ferroelectric layer during the removal of PS nanoparticles or a mechanical damage while contacting the device with the electrodes.

5.8.2 Combined optical - electrical measurements

After this step a sequence of optical spectra are acquired while applying different voltages. We call (+) polarization the one reached by the material when the positive electrode is on the nanodisks side and $V > V_{Th}$ is applied. We call (-) polarization the opposite situation. Initially a ramp of different voltages were applied to the samples, monitoring the result in terms of position of different peaks, with different polarization direction of the material. Data from the spectrometer and from the Keithley 2400 are temporally correlated, to observe the changes in peak position related to different voltages applied. In Fig.5.11 we can observe, for example, two trends of the 700 nm well for different polarized samples.

The effect can be explained as a Fabry Perot cavity resonance shift due to

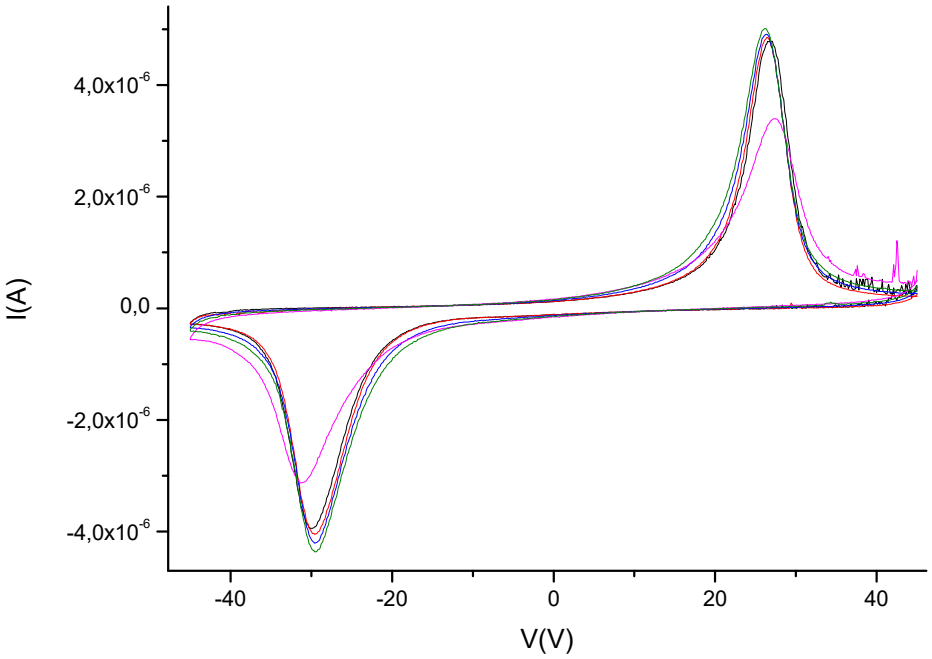

Figure 5.10: IV curves acquired during the poling process. The curves are acquired after four cycles. One cycle lasts 60 s and consists in a circular sweep from -60V to 60V. The response obtained is reproducible.

reverse piezoelectric effect. The voltage cause a strain in the material that leads to a linear deformation. The cavity mode is than shifted due to the different width of the cavity.

The piezoelectric coefficient for P(VDF-TrFE) is -31.4 pm V^{-1} [Kat+16]. The negative sign confirm the observed behaviour, with reduction in length, when negative voltage is applied. For $\Delta V = 40V$, the expected shifts in the resonance are: -3.41 nm, -1.71 nm, -1.41 nm (for n=1,2,3 modes). The shift value is confirmed by Fig.5.11 for the third mode of the cavity, close to 700nm. The other peaks show a related trend, but the 900 nm peak does not show the expected shift.

From Fig.5.12 it is possible to notice that 1) The peak value at 0 V is not the same for the two polarizations, 2) the value at 40 V is not the same before and after the sweep.

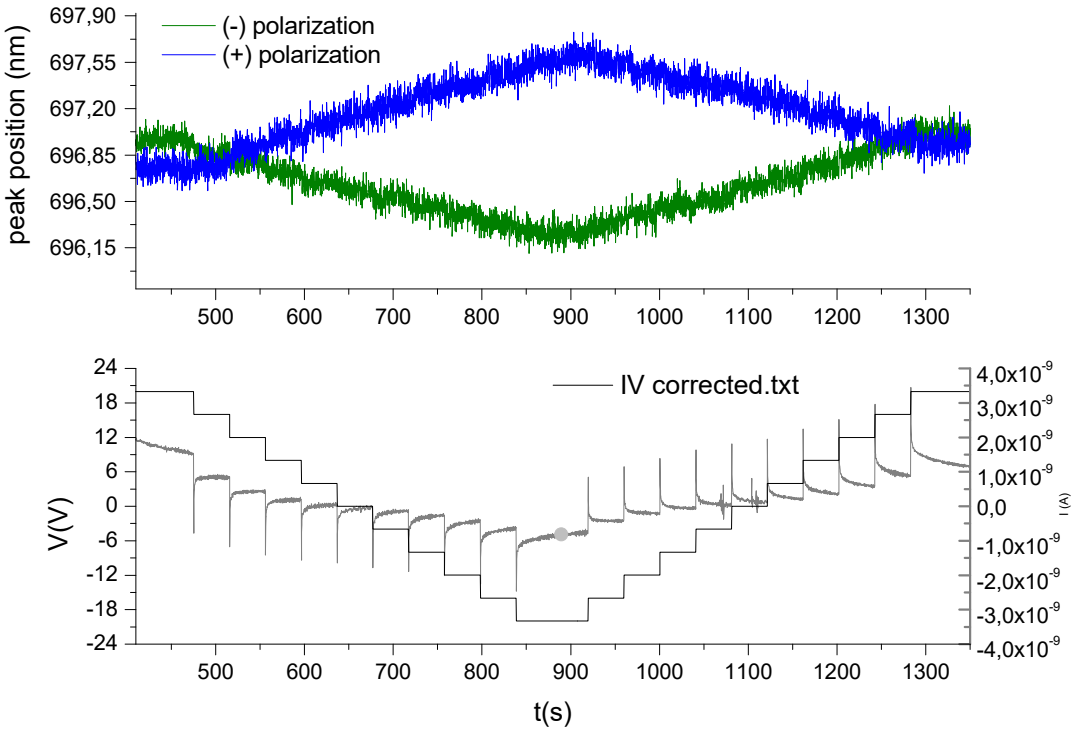

Figure 5.11: (top) Trend of the peak position while applying a sweep in voltage from +20V to -20V and back. The sweep is not changing the polarization of the device. (-) polarization means the polarization obtained with a voltage of 60V with negative electrode on the nanodisks side, while (+) polarization means the one obtained with positive electrode on nanodisks side. Each behaviour of peak position, for different polarizations, is compatible with the cavity stretching effect. With (-) polarization the cavity reduces when negative voltage is applied while expands when positive voltage is applied. For (+) polarization the behaviour is opposite. The different value at V=0 and the differences for V=20 before and after the sweep are not compatible only with that phenomena. (bottom): voltage applied to the sample, with positive electrode on nanodisks substrate. The light gray signal is the current recorded by Keithley 2400 while applying voltage.

To investigate in more details this observations other type of measurements are required. The first measurement wants to determine the relaxation time when a new polarization state is reached. A sweep form -45 V to +45 volts is performed, then constant +45 V voltage is left. After the polarization the peak position decays exponentially to a lower value. An exponential fit is performed on that segment

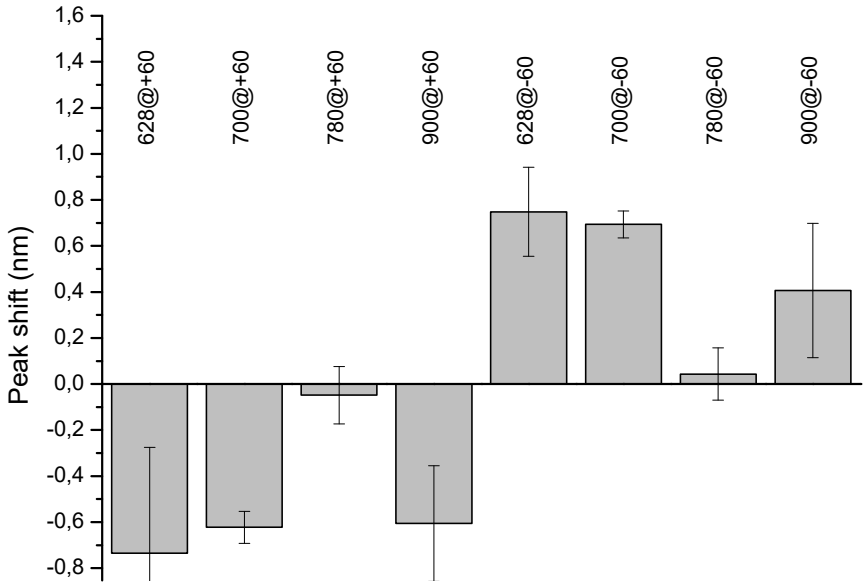

Figure 5.12: Peak shift between +20V and -20 V applied on samples with nanodisks. The error bar derives from the fit on the peak value in the interval where the voltage was constant. It is possible to see that the shift for the 630 nm, 700nm and 900 nm is cohered with the cavity stretching effect. The peak at 780 nm instead doesn't show any shift.

and reveals a decay time of 98 s, as shown in Fig.5.13.

In the next type of measurements we want to observe the effects of different polarization with no electrical stimulation, in order to avoid Fabry Perot stretching effect.

Measurements were performed switching alternatively the voltage in this sequence: -45 V, 0 V, +45 V, 0 V. In this way different polarizations where set and the optical effect on the sample with no stimulation is analyzed. The acquisition time for each voltage was 120 s, to get significant time to get the exponential fit on the different peak steps but not too long to observe intensity instabilities from the lamp. The measures were performed with 10 S/s sampling frequency. The results are shown in Fig.5.14.

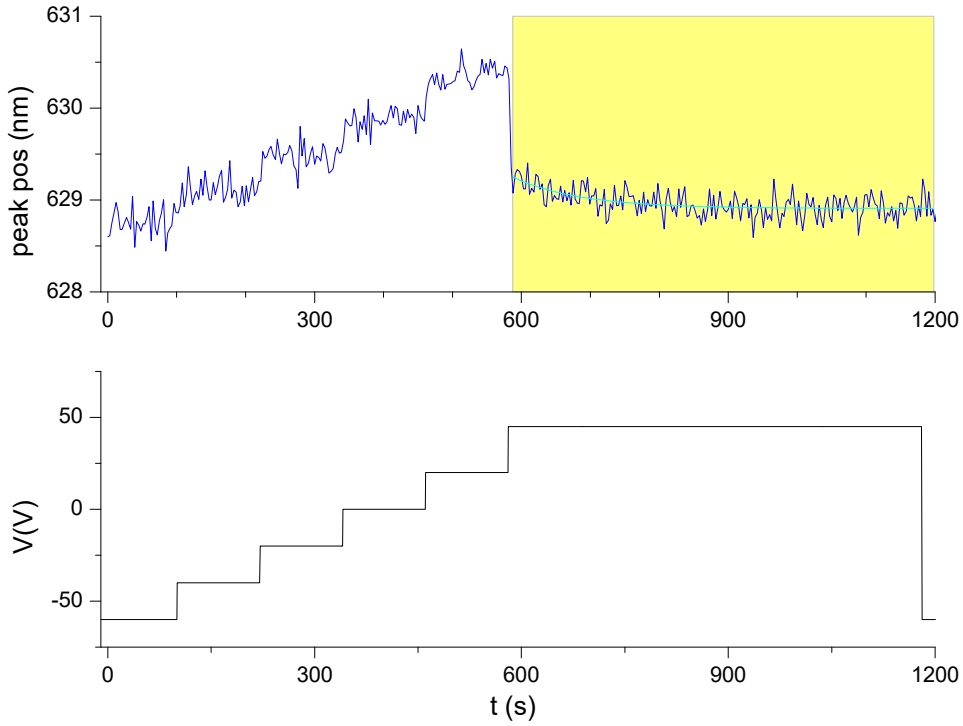

Figure 5.13: The measure describes the evolution of the optical response after changing polarization. It is possible to observe an exponential decay with time constant 98 s. After the polarization a the peak drops, than an exponential decay make the peak value stable.

The Fabry Perot cavity stretching is the same for +45 V and -45 V applied because opposite polarization with opposite electrical stimulation give the same deformation.

The results are compatible with the FP effects for the peaks at 700 nm, 630 nm, 530 nm. For the peak at 780 nm and 900 nm the behaviour instead is different. We notice a difference in the two polarization states when the voltage is set to 0.

Data is better described in Fig. 5.15, where the peak position is averaged and fitted over 7 cycles. The error bar is given by the standard deviation of the fitted values. Only the peak at 790 nm shows two incompatible values for two different polarizations and 0 V applied, that remands to a polarization effect on the optical proprieties of the sample.

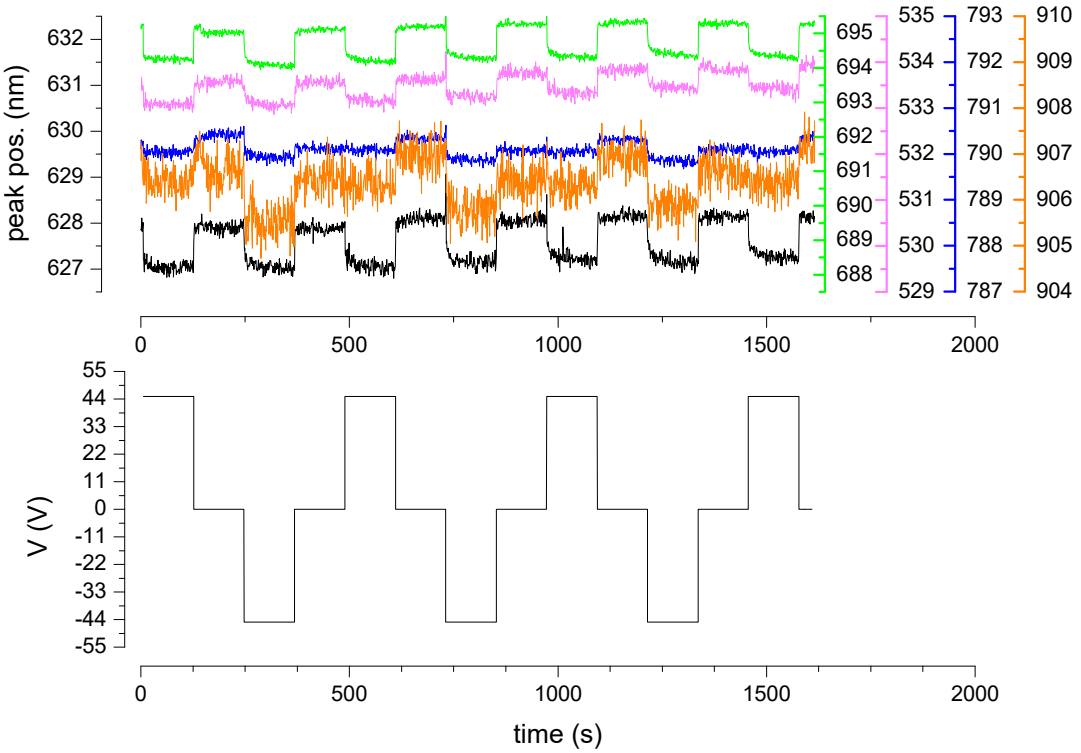

Figure 5.14: The temporal evolution of different peaks is described in the graph on top, correlated to the evolution of the applied voltage. Each step in voltage lasts 120 s, and it is possible to observe differences in optical response between two polarization states for peaks at 900 nm and 780 nm.

The result is opposite than expectations from theory. Applying positive voltage to the nanodisks we induce a polarization that flips the dipoles of the ferroelectric material to create a positive surface charge on the nanodisks. The theory says that a lack of electrons in the material cause a redshift, but here the peak wavelength is lower than the case with opposite polarization.

It is also important to notice that electrical stimulation and optical measurements are uncoupled. The data is then reliable because the electrical stimulation can not influence in other ways the optical part.

The analysis were performed, for the sequential stimulation with +45V, 0V, -45V, 0V also measuring spectra in reflection. From Fig. 5.16 it is possible to observe that the signal presents instabilities in the peak position, that is why

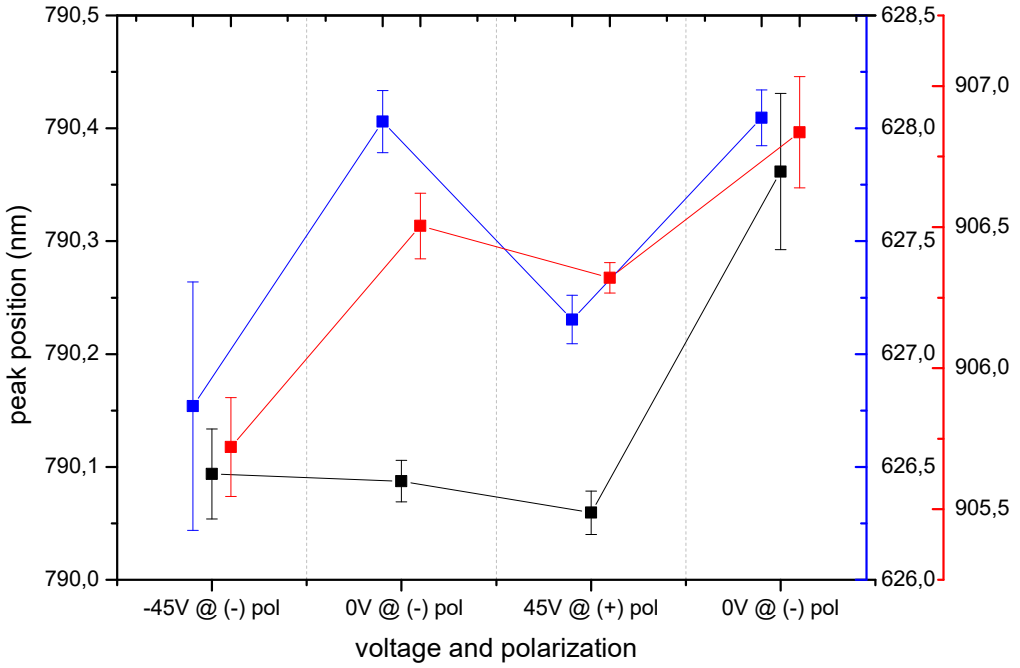

Figure 5.15: Different peak position for different voltages applied and polarizations of the material. Error bars are obtained as standard deviations from 10 different data obtained fitting curves in Fig. 5.14. To notice that only peaks at 790 nm and 900 nm present differences for different polarizations with 0V applyed. The differences are, respectively, 0.27 nm and 0.33 nm.

the peak position statistics were not performed in this case. From the graph it is possible to observe that the peak at 700 nm follows the FP cavity stretching effect, but it is present a little spike in the signal when the material is polarized in different directions. The spike is related to the spike in current due to the polarization, so it can be caused by a thermal effect that changed the refractive index of the surrounding material. The duration of the spike in less than 100 ms and it is too short to be analyzed with our acquisition system.

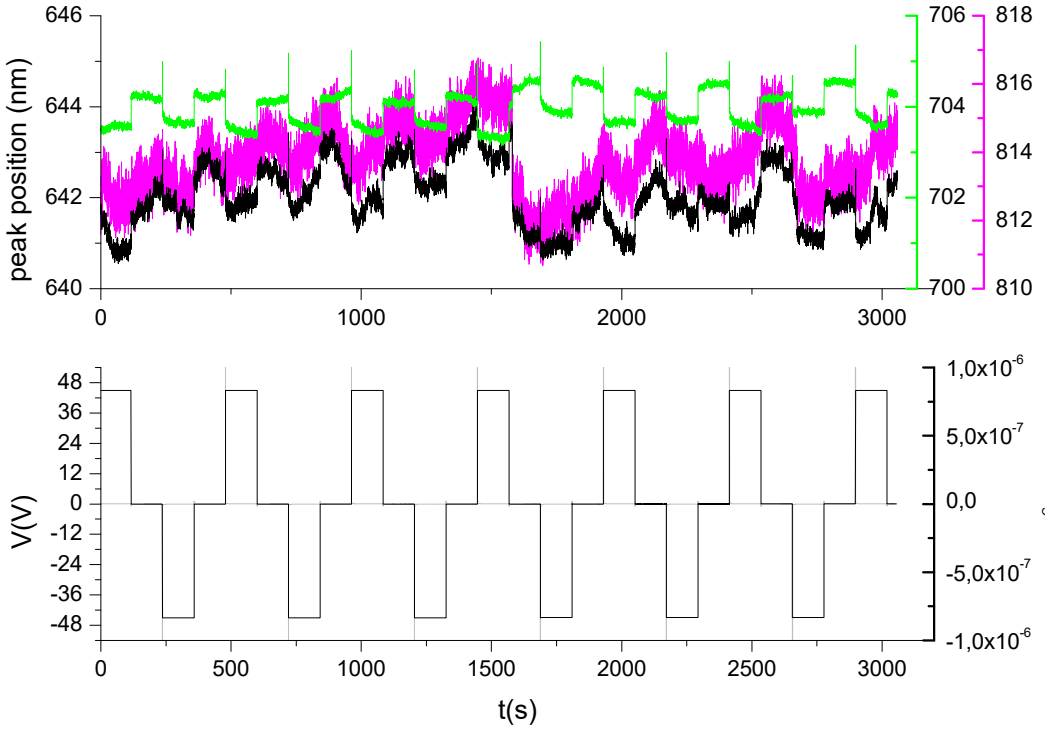

Figure 5.16: The temporal evolution of different peaks for reflection spectra is described on top, correlated to the evolution of the applied voltage. Each step in voltage lasts 120". It is possible to notice that the 704 nm peak follow Fabry Perot cavity effect, while other peaks shows instabilities and not clear trend. When the polarization is switched the peak position is showing a spike, redshifting. This effect can be caused by a variation in the refractive index of the material through the polarization current flowing in the device.

5.9 Samples with nanoholes

Hybrid plasmonic-ferroelectric devices were used to investigate the polarization dependence of the LSPR. In the previous section we showed the results for devices composed by gold nanodisks coupled to ferroelectric P(VDF-TrFE).

The results show that a Fabry Perot cavity effect is present. While applying voltage to polarize the device, the inverse piezoelectric effect stretches the cavity and modifies the resonance.

If a shift by the stretching of the cavity is present, then it is not possible to

observe plasmonic resonance shift just after polarizing the material .

We decided to produce and study another type of devices to avoid the Fabry Perot cavity effects. The device is composed by two electrodes: one made of ITO and the other one made of gold thin film with nanoholes. In the samples reflectivity of ITO is low and the Fabry Perot cavity effect is less visible.

For the samples with nanoholes many failures occurred. All the samples produced, after a few cycles of electrical stimulation, failed, showing high currents and unpredictable optical behaviour.

For this samples the analysis was restricted to the electrical stimulation with +40V, 0V, -40V, 0V to investigate directly the modifications in the peaks with different polarizations.

The peak position were monitored in extinction in 530 nm and in 770 nm (plasmonic effect). The trend, as we can see in Fig. 5.17, is not stable and this behaviour happened during all the measurements, probably due to structural cracks in the device, allowing an unstable but high (μA) current to flow through the sample.

From measurements in Fig. 5.17 we derived the statistics on the peaks position but, due to the instability of the peak value in time, we averaged only a portion of data that are compatible. Results (Fig. 5.18) show an opposite behaviour for the two peaks observed. The peak at 775 nm behaves coherently with the Fabry Perot stretching effect.

The unstable behaviour is caused by the defects on the ferroelectric layer. We suppose that the defects are caused by the removal of the nanoparticles by sticking them with a gel layer. This gel can sticks also to the metal film, due to the low density of nanoparticle, causing cracks or deformations.

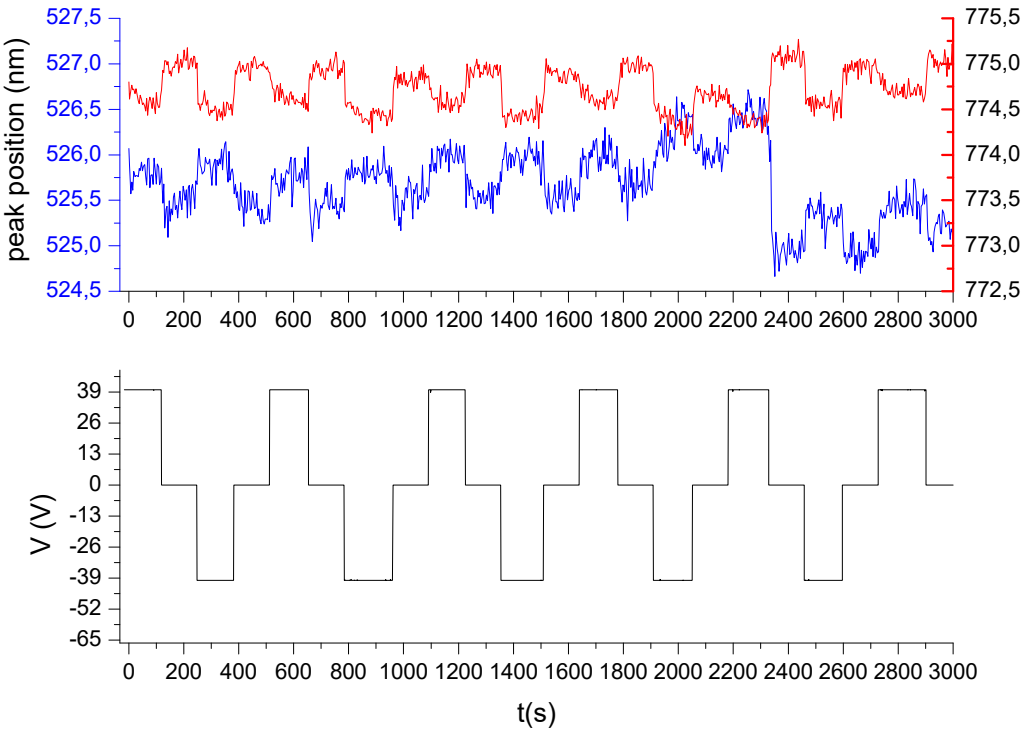

Figure 5.17: Computed peak value related to the electrical signal applied. The measured samples have a ferroelectric layer with two electrodes, one made by ITO and the other by gold film with nanoholes. Comparing to the devices with nanodisks, the signal is less stable and is subject to fluctuation that makes the analysis less reliable. It is possible to observe different and opposite behaviour for the two observed peaks.

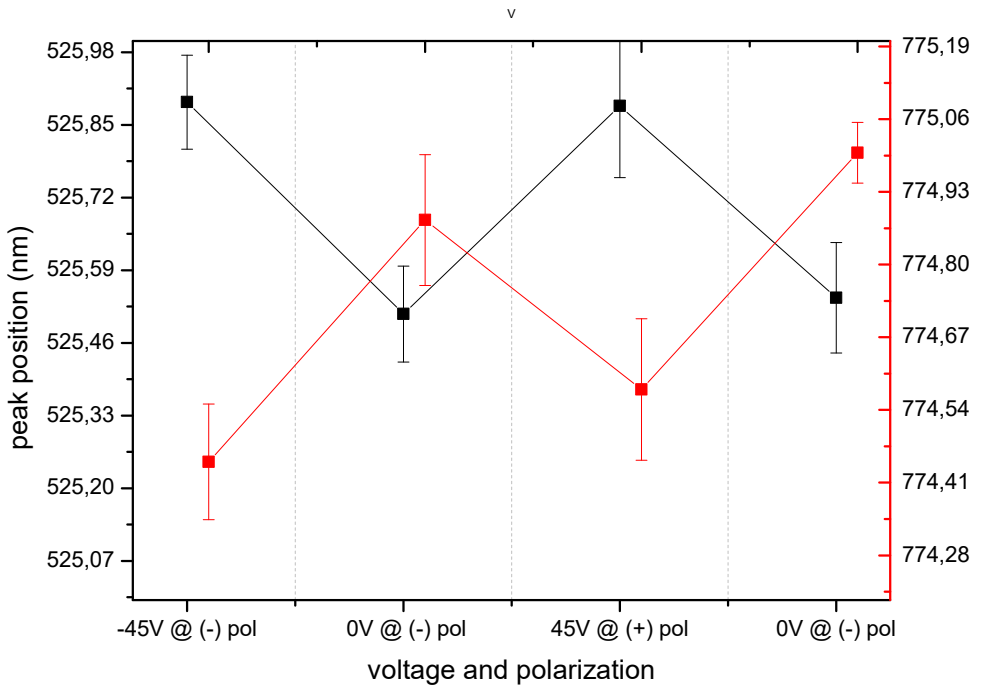

Figure 5.18: Different peak position for different voltages applied and polarizations of the material. Error bars are obtained as standard deviations from 10 different data. This data derives from fitting the peak position function in the interval where constant voltage is applied. To avoid the instability obtained in the peak signal the used signal is restricted to an area where the values are compatible, before an offset. To notice the different result in the shift for two monitored peaks.

Part V

Conclusions

In this works the influence of coupling a ferroelectric polarized material with nanostructures supporting localized surface plasmonic resonance was investigated.

To perform this study, the optical proprieties of coupled ferroelectric-plasmonic devices has been analyzed.

Initially, a LabView program was written to acquire time correlated data from a spectrometer and a source-meter. The program overcome the limitation of the predefined spectrometer program of acquiring limited number of spectra. The program is capable also to compute the acquired data to obtain the shift in time of various peaks of the spectrum.

After that plasmonic-ferroelectric devices were produced in cleanroom. The different devices were based on gold nanodisks and gold nanoholes structures. The first type of device presents a layer of ferroelectric P(VDF-TrFE) placed between a layer of gold nanodisks and a gold thin film. The second type of device presents the ferroelectric layer between a layer of ITO and a gold thin film with nanoholes. The production were performed using the techniques of spin coating, to produce the ferroelectric polymeric film, of physical vapor deposition, to produce thin films and of colloidal lithography to produce nanodisks and nanoholes. The results show a better short range order in gold nanodisks than for nanoholes.

The devices were optically characterized measuring the spectra in reflection and in transmission. The different spectra were compared with the spectra of control devices to recognize the peaks related to different phenomena. We also compared the measured spectra with simulated spectra obtained by finite difference frequency domain simulations. The simulations partially confirm the observed behaviour. A Fabry- Perot cavity effect was found and a localized surface plasmonic resonance can be associated to a peak in extinction of gold nanodisks .

The samples were electrically stimulated, to alternately change the polarization of the ferroelectric material. At the same time either the transmission or the reflection spectra of the sample were captured. The peak position was then computed for each spectra using a centroid method. This method calculate the barycenter of a portion of the acquired spectra containing a peak.

From this measurements a correlation were noticed between the electrical stimulation and the optical response in terms of peak position. The first observed effect was a cavity stretching due to inverse piezoelectric phenomena. This effect cause

a shift in the peaks of the Fabry Perot cavity when a voltage was applied. The observed shifts are compatible with expected values.

The second observed effect is a difference in the extinction peak of gold nanodisks, between different polarization states of the interfaced ferroelectric material. It can be caused by differences in refractive index of the material in the two polarization states or by the surface charge that is interfaced to the nanodisks. Following a Drude-based theoretical treatment the shift was opposite to the expected value.

After polarizing the material in different directions, a spike in the reflection spectrum peak position was observed. It can be caused by thermal effects of the polarization current.

In conclusion we can state that a difference in the localized surface plasmonic resonance, due to the polarization state of an interfaced ferroelectric material were observed. The limitation of this study resides on the device characteristics that can not completely avoid a Fabry Perot cavity resonance. To overcome this limitation the device used to observe this phenomena should be transparent near the plasmonic resonance wavelength, leaving the plasmonic phenomena more evident. Another limitation for looking at transitory phenomena is the sampling speed of the spectrometer. This speed is mainly limited by the exposure time required by the camera, that can be reduced using more powerful light source coupled with neutral filter for reference signal, or a different spectrometer.

Concerning the device production the main problem for nanoholes devices, made to avoid Fabry Perot cavity effects, was the critical removal of nanoparticles from the top layer, cause of failures. To avoid this problem it is more reliable to perform the fabrication of nanodisks or nanoholes on a robust substrate, like ITO layer or glass, instead of delicate P(VDF-TrFE) film.

Bibliography

[13] *Piezoelectric Polymers*. http://www.physics.montana.edu. Accessed: 2019-01-21. 2013 (cit. on p. 22).

[19] *Refractive index database*. https://refractiveindex.info/. Accessed: 2019-01-21. 2019 (cit. on p. 43).

[BH83] C. F. Bohren and D. R. Huffman. *Absorption and Scattering of Light by Small Particles*. Wiley-VCH, 1983. ISBN: 9780471293408 (cit. on p. 14).

[BW99] M. Born and E. Wolf. *Principles of Optics*. 7th ed. Cambridge University Press, 1999 (cit. on pp. 10, 11).

[DKD16] A. Derkachova, K. Kolwas, and I. Demchenko. "Dielectric function for gold in plasmonics applications: size dependence of plasmon resonance frequencies and damping rates for nanospheres". In: *Plasmonics* 11.3 (2016), pp. 941–951 (cit. on p. 11).

[Dru00] P. Drude. "Zur Elektronentheorie der Metalle". In: *Annalen der Physik* 306 (1900), pp. 566–613. DOI: 10.1002/andp.19003060312 (cit. on p. 10).

[DTH06] A. B Dahlin, J. O. Tegenfeldt, and F. Höök. "Improving the instrumental resolution of sensors based on localized surface plasmon resonance". In: *Analytical chemistry* 78.13 (2006), pp. 4416–4423 (cit. on p. 40).

[FDF80] T. Furukawa, M. Date, and E. Fukada. "Hysteresis phenomena in polyvinylidene fluoride under high electric field". In: *Journal of Applied Physics* 51.2 (1980), pp. 1135–1141 (cit. on p. 22).

[Fre+07] H. Fredriksson et al. “Hole–mask colloidal lithography”. In: *Advanced Materials* 19.23 (2007), pp. 4297–4302 (cit. on p. 24).

[FSJ14] J. A. Faucheaux, A. L. D. Stanton, and P. K. Jain. “Plasmon resonances of semiconductor nanocrystals: Physical principles and new opportunities”. English. In: *Journal of Physical Chemistry Letters* 5.6 (2014). Cited By :126, pp. 976–985. URL: www.scopus.com (cit. on p. 8).

[He+16] J. He et al. “Near-field engineering of Fano resonances in a plasmonic assembly for maximizing CARS enhancements”. English. In: *Scientific Reports* 6 (2016). Cited By :23. URL: www.scopus.com (cit. on pp. 8, 15).

[HH85] E. J. Heilweil and R. M. Hochstrasser. “Nonlinear spectroscopy and picosecond transient grating study of colloidal gold”. English. In: *The Journal of chemical physics* 82.11 (1985). Cited By :160, pp. 4762–4770 (cit. on p. 15).

[HKS03] P. Hanarp, M. Käll, and D. S. Sutherland. “Optical properties of short range ordered arrays of nanometer gold disks prepared by colloidal lithography”. English. In: *Journal of Physical Chemistry B* 107.24 (2003). Cited By :277, pp. 5768–5772 (cit. on p. 16).

[Jac99] John David Jackson. *Classical electrodynamics*. 3rd ed. Wiley, 1999. ISBN: 9780471309321 (cit. on p. 12).

[Jul+08] B. K. Juluri et al. “Effects of geometry and composition on charge-induced plasmonic shifts in gold nanoparticles”. English. In: *Journal of Physical Chemistry C* 112.19 (2008). Cited By :63, pp. 7309–7317 (cit. on p. 17).

[Kat+16] I. Katsouras et al. “The negative piezoelectric effect of the ferroelectric polymer poly (vinylidene fluoride)”. In: *Nature materials* 15.1 (2016), p. 78 (cit. on pp. 22, 55).

[Kaw69] Heiji Kawai. “The piezoelectricity of poly (vinylidene fluoride)”. In: *Japanese Journal of Applied Physics* 8.7 (1969), p. 975 (cit. on p. 21).

[Lam+00] B. Lamprecht et al. “Metal Nanoparticle Gratings: Influence of Dipolar Particle Interaction on the Plasmon Resonance”. In: *Physical Review Letters* 84.20 (2000). Cited By :482, pp. 4721–4724 (cit. on pp. 15, 16).

[Lar+09] E. M. Larsson et al. “Nanoplasmonic probes of catalytic reactions”. English. In: *Science* 326.5956 (2009). Cited By :269, pp. 1091–1094. URL: www.scopus.com (cit. on p. 8).

[Lio+14] C. Liow et al. “Dependence of plasmonic properties on electron densities for various coupled Au nanostructures”. English. In: *Journal of Physical Chemistry C* 118.47 (2014). Cited By :13, pp. 27531–27538 (cit. on p. 17).

[Liu+10] N. Liu et al. “Planar metamaterial analogue of electromagnetically induced transparency for plasmonic sensing”. English. In: *Nano Letters* 10.4 (2010). Cited By :726, pp. 1103–1107. URL: www.scopus.com (cit. on p. 8).

[LKZ07] C. Langhammer, B. Kasemo, and I. Zorić. “Absorption and scattering of light by Pt, Pd, Ag, and Au nanodisks: Absolute cross sections and branching ratios”. English. In: *Journal of Chemical Physics* 126.19 (2007). Cited By :144 (cit. on p. 16).

[LLH07] S. Lal, S. Link, and N. J. Halas. “Nano-optics from sensing to waveguiding”. English. In: *Nature Photonics* 1.11 (2007). Cited By :1547, pp. 641–648. URL: www.scopus.com (cit. on p. 8).

[Luk+10] B. Luk’Yanchuk et al. “The Fano resonance in plasmonic nanostructures and metamaterials”. English. In: *Nature Materials* 9.9 (2010). Cited By :2186, pp. 707–715. URL: www.scopus.com (cit. on p. 8).

[Mai+02] S. A. Maier et al. “Observation of near-field coupling in metal nanoparticle chains using far-field polarization spectroscopy”. English. In: *Physical Review B - Condensed Matter and Materials Physics* 65.19 (2002). Cited By :353, pp. 1934081–1934084 (cit. on p. 15).

[Mai07] Stefan Alexander Maier. *Plasmonics: Fundamentals and Applications*. 1st ed. Springer, 2007. ISBN: 0387331506 (cit. on pp. 13, 14).

[Mul+06] P. Mulvaney et al. “Drastic surface plasmon mode shifts in gold nanorods due to electron charging”. English. In: *Plasmonics* 1.1 (2006). Cited By :112, pp. 61–66 (cit. on p. 17).

[NE97] S. Nie and S. R. Emory. “Probing single molecules and single nanoparticles by surface-enhanced Raman scattering”. English. In: *Science* 275.5303 (1997). Cited By :7626, pp. 1102–1106. URL: www.scopus.com (cit. on p. 8).

[OCH06] K. M. Ok, E. O. Chi, and P. S. Halasyamani. “Bulk characterization methods for non-centrosymmetric materials: Second-harmonic generation, piezoelectricity, pyroelectricity, and ferroelectricity”. English. In: *Chemical Society Reviews* 35.8 (2006). Cited By :457, pp. 710–717 (cit. on p. 20).

[Pit+07] J. M. Pitarke et al. “Theory of surface plasmons and surface-plasmon polaritons”. English. In: *Reports on Progress in Physics* 70.1 (2007). Cited By :753, pp. 1–87 (cit. on p. 13).

[Rua+18] L. Ruan et al. “Properties and Applications of the β Phase Poly (vinylidene fluoride)”. In: *Polymers* 10.3 (2018), p. 228 (cit. on p. 21).

[Shi+18] M. Shiran Chaharsoughi et al. “Hybrid Plasmonic and Pyroelectric Harvesting of Light Fluctuations”. In: *Advanced Optical Materials* (2018), p. 1701051 (cit. on pp. 16, 24, 25, 46, 47).

[ST19] Bahaa EA Saleh and Malvin Carl Teich. *Fundamentals of photonics*. john Wiley & sons, 2019 (cit. on p. 19).

[Ueb01] Pierre Ueberschlag. “PVDF piezoelectric polymer”. In: *Sensor review* 21.2 (2001), pp. 118–126 (cit. on p. 22).

[Wan+06] D.Y. Wang et al. “Optical characterization of P (VDF-TrFE) copolymer films by the prism coupling technique”. In: *Integrated Ferroelectrics* 78.1 (2006), pp. 199–206 (cit. on pp. 43, 48).

[WH76] Yasaku Wada and Reinosuke Hayakawa. “Piezoelectricity and pyroelectricity of polymers”. In: *Japanese Journal of Applied Physics* 15.11 (1976), p. 2041 (cit. on p. 21).

[Zor+11] I. Zorić et al. “Gold, platinum, and aluminum nanodisk plasmons: Material independence, subradiance, and damping mechanisms”. English. In: *ACS Nano* 5.4 (2011). Cited By :241, pp. 2535–2546 (cit. on p. 16).